ELSEVIER

Coordination Chemistry Reviews
159 (1997) 325–358

COORDINATION CHEMISTRY REVIEWS

Low-lying electronic states of $[Rh(bpy)_3]^{3+}$, $[Pt(bpy)_2]^{2+}$, and $[Ru(bpy)_3]^{2+}$. A comparative study based on highly resolved and time-resolved spectra

Hartmut Yersin *, Werner Humbs, Johann Strasser

Institut für Physikalische und Theoretische Chemie, Universität Regensburg D-93040, Regensburg, Germany

Received 22 December 1995

Contents

* Corresponding author.

PII S0010-8545(96)01318-5

Abstract

Optical emission and excitation spectra of $[Rh(bpy\text{-}h_8)_3]^{3+}$, $[Rh(bpy\text{-}h_8)_2(bpy\text{-}d_8)]^{3+}$, $[Rh(bpy\text{-}d_8)_3]^{3+}$, $[Pt(bpy\text{-}h_8)_2]^{2+}$, $[Pt(bpy\text{-}h_8)(bpy\text{-}d_8)]^{2+}$, $[Pt(bpy\text{-}d_8)_2]^{2+}$, $[Ru(bpy\text{-}h_8)_3]^{2+}$, $[Ru(bpy\text{-}h_8)_2(bpy\text{-}d_8)]^{2+}$, and $[Ru(bpy\text{-}d_8)_3]^{2+}$ are discussed. A series of trends—also including $[Os(bpy)_3]^{2+}$—is uncovered. These trends, which are connected with an increase in metal-d or MLCT character in the lowest triplet states, can for instance be seen in transition energies, emission lifetimes, zero-field splittings, rates of spin–lattice relaxation, vibronic satellite structures, and changes of nuclear equilibrium positions on excitation. Moreover, the compounds investigated are also appropriate for consideration of the concept of "dual emission", the relation between MLCT character and covalency, as well as the current models of localization/delocalization. In particular, a comparison of the properties of $[Rh(bpy)_3]^{3+}$- and $[Ru(bpy)_3]^{2+}$-doped $[Zn(bpy)_3](ClO_4)_2$ provides illustrative and very strong evidence for covalent delocalization in the lowest excited states of $[Ru(bpy)_3]^{2+}$, while ligand-centered localization is found in the states of $[Rh(bpy)_3]^{3+}$. Misinterpretations might occur if the aggregation effects of the chromophores are not taken into account. © 1997 Elsevier Science S.A.

Keywords: MLCT character; Highly resolved spectra; Time resolved spectra

1. Introduction

Transition metal complexes with organic ligands have been investigated with increasing interest over the last decades, since these complexes exhibit an enormous potential for the discovery of new physical and chemical properties, and applications. For example, supramolecular chemistry involving transition metal complexes as subunits represents an important, rapidly developing field [1,2]. Moreover, photo-redox processes for solar energy conversion [3–5], information storage systems [6], laser materials [7], biosensors [8], and complexes with antitumor activity [9–11] have already been explored or are currently under investigation [12,13]. Most of the possible applications are related to the properties of the lowest excited electronic states. Consequently, these states should be studied in more detail. In particular, they exhibit a series of not yet well-known electronic properties, which are found neither in already well-studied, pure organic molecules (see, for example, Ref. [14]) nor in simple metal complexes with d–d* transitions (see, for example, Refs. [15], [16] and [17]). For example, the lowest excited states of $[Rh(bpy)_3]^{3+}$ can be classified as ligand centered (LC) of (bpy)$\pi\pi^*$ character (bpy: 2,2′-bipyridine), although slightly distorted by the metal [18], while those of $[Ru(bpy)_3]^{2+}$ result from metal-to-ligand charge-transfer (MLCT) transitions of Ru4d-bpyπ^* character [4,5,12,13,18–21]. These two types of transition may be regarded as two extreme situations, which lead to distinctly different physical properties of the corresponding compounds. Interestingly, complexes are also found, such as the series of ortho-metalated Pt(II) compounds, which belong to an intermediate situation. Thus, the question arises as to whether it is possible to characterize such a situation more precisely. At present, computational quantum chemical

methods do not seem to be sufficiently powerful for a reliable description of excited triplet states in systems with such a large number of electrons. However, an experimental approach based on spectroscopy should be successful, if the spectroscopic information is sufficiently detailed. This is mostly not the case, since only broad and unresolved spectra are available.

Recently, a detailed characterization of the lowest excited states of a series of ortho-metalated Pd(II) and Pt(II) compounds was achieved, based on highly resolved emission and excitation spectra [22–25]. Indeed, it was possible to develop criteria which, for example, allow to characterize an increasing MLCT or metal-d admixture to the ^{3}LC states. This can be achieved by using (i) the energy position of the lowest triplet, (ii) its zero-field splitting (ZFS) into sublevels, (iii) the longest component of the emission lifetime, and (iv) the spectrally well-resolved vibrational satellite structures, which carry a huge amount of information [26,27].

It is the aim of this review to focus on the properties of the lowest excited states (and ground states) of metal complexes with bpy ligands. A characterization in the sense of the criteria mentioned is only possible if highly resolved spectra are available, as is the case for $[Rh(bpy)_3]^{3+}$, $[Pt(bpy)_2]^{2+}$, $[Ru(bpy)_3]^{2+}$, and $[Os(bpy)_3]^{2+}$ (see below for references). The extensive information displayed in these resolved spectra is used not only to characterize and compare their properties, but also to address the problems which have arisen during the investigation of these compounds, such as the puzzle of localization/delocalization, the shifts of nuclear equilibrium positions on excitation, the possible occurrence of a dual emission, the time scales of intra- or intermolecular processes, and simplifications connected with a one-electron model of MLCT transitions. Most of these problems can be discussed much more rigorously on the basis of a comparative study.

2. $[Rh(bpy)_3]^{3+}$

Fig. 1 illustrates the optical properties of $[Rh(bpy)_3]^{3+}$, showing absorption and emission spectra measured with a usually obtainable resolution (see also Refs. [28],

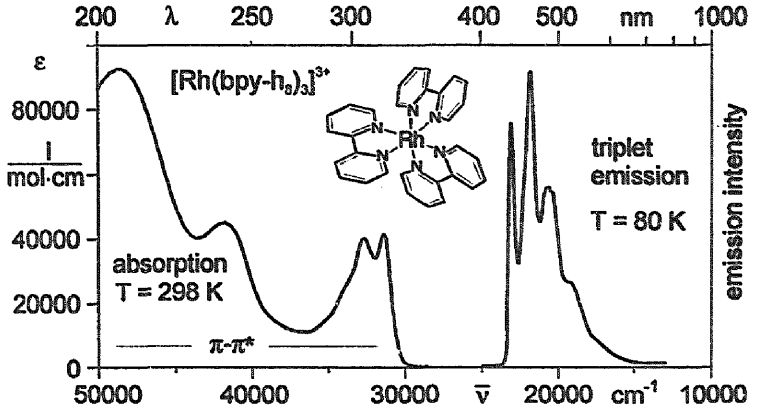

Fig. 1. Ordinary absorption and emission spectra of $[Rh(bpy)_3]^{3+}$ dissolved in ethanol (λ_{exc} = 320 nm).

[29], [30] and [31].) The various strong transitions observed in the absorption spectrum below 350 nm are generally assigned to $\pi\pi^*$ LC singlet–singlet transitions [28–31]. An individual ligand interacts with the other ligands via the coupling of transition dipole moments, which may be described in a "molecular exciton model" [32–36]. Even if orbital overlap and admixture with d-orbitals of the metal ion are neglected, these dipole–dipole interactions may be relatively strong for strongly allowed electric dipole transitions (in the order of several $10^2\,cm^{-1}$ [34–36]). Consequently, these singlet states belong to the whole ligand system.

In this contribution, we are mainly interested in the lowest triplet state(s) T_1. The corresponding absorption from the singlet ground state S_0 is relatively weak. Thus, the "exciton model" as discussed above is not applicable to the triplet(s) [33]. In most contributions, the transition $S_0 \rightarrow T_1$ is regarded as being confined to one bpy ligand and is assigned to mainly $\pi\pi^*$ parentage [28–31,37–42]. This will also be demonstrated in Section 2.2. (Compare the related papers of Güdel and co-workers [43–45].) Fig. 1 shows the emission from the lowest triplet, and it is seen that T_1 lies at a much lower energy than the lowest singlet S_1, mainly because of the exchange interaction. A more detailed discussion of this rather broad emission spectrum does not seem to be reasonable, but see Section 2.2.

2.1. $[Rh(bpy)_3]^{3+}$ in crystalline $[Zn(bpy)_3](ClO_4)_2$

Very often it is not possible to obtain highly resolved optical spectra from a neat material, because of broadening of the spectra due to, for example, energy transfer, inhomogeneity effects, and electron phonon coupling. Thus, the technique of doping

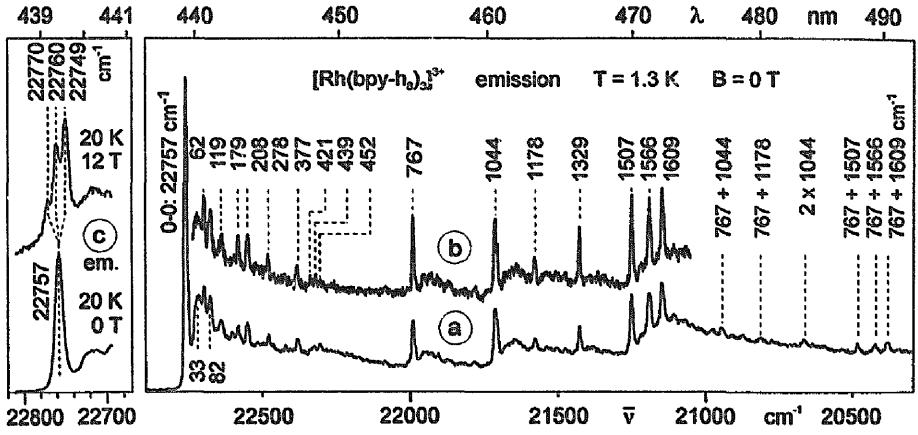

Fig. 2. Highly resolved and line-narrowed emission of $[Rh(bpy\text{-}h_8)_3]^{3+}$ in $[Zn(bpy\text{-}h_8)_3](ClO_4)_2$ (see Ref. [42]). The excitation energy for (a) and (c) was $\bar{\nu}_{exc}=29\,665\ cm^{-1}$ ($\triangleq$337.1 nm), and for the line-narrowed spectrum (b) was $\bar{\nu}_{exc}=22\,757\ cm^{-1}$ ($S_0 \rightarrow T_1$, resonantly excited). The crystals were grown from water/acetone (1:4) with a solution molar ratio Rh(III):Zn(II) of 1%. The energies of the satellites are specified relative to the electronic origin at 22 757 cm^{-1}. (c) shows the region of the origin(s) on an enlarged scale for $B=0$ T and $B=12$ T, respectively ($T=20$ K).

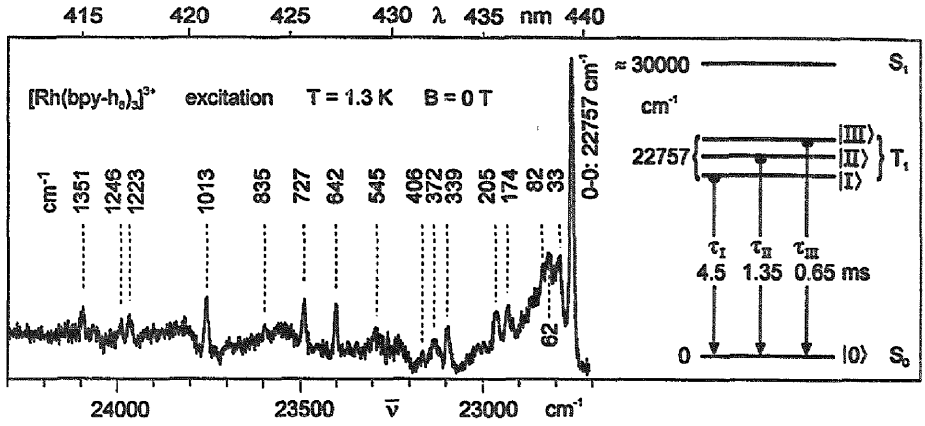

Fig. 3. Excitation spectrum of $[Rh(bpy\text{-}h_8)_3]^{3+}$ in $[Zn(bpy\text{-}h_8)_3](ClO_4)_2$ (see Ref. [42]). Detection energy at $\bar{\nu}_{det}$=21 148 cm^{-1} ($\triangleq$1609 cm^{-1} satellite). Inset: the energy level scheme for the lowest triplet T_1 and the singlet S_1, as well as the emission decay times. For further data see Fig. 2.

transition metal complexes with organic ligands in suitable crystalline matrices with low doping concentrations has often been applied [21–27,42–45]. Indeed, this procedure is also successful for the doping of $[Rh(bpy)_3]^{3+}$ guests into a crystalline $[Zn(bpy)_3](ClO_4)_2$ host. This host material is photophysically inert in the spectral region of interest. Owing to the different charges of the Rh(III) and Zn(II) complexes, the dopants are not expected to symmetrically substitute the host molecules. Therefore, the site symmetries of the guests cannot be specified. Moreover, the molar concentration of, for example, 1% Rh(III):Zn(II) in solution will presumably not be maintained in the doped crystals. It is even more likely that $[Rh(bpy)_3]^{3+}$ is not statistically built into the lattice and that regions of enriched dopants occur (see also Section 4.1). Nevertheless, the low-temperature spectra obtained for $[Rh(bpy)_3]^{3+}$ are about 100-fold better resolved [42] than those previously published.

2.2. *Characterization of the lowest triplet of* $[Rh(bpy\text{-}h_8)_3]^{3+}$

Figs. 2 and 3 reproduce the low-temperature emission and excitation spectra of $[Rh(bpy\text{-}h_8)_3]^{3+}$-doped crystalline $[Zn(bpy\text{-}h_8)_3](ClO_4)_2$ (from Ref. [42]). These spectra display much information, as will be discussed in detail in the following sections.

2.2.1. *Electronic origins and triplet sublevels*

The dominating line in the emission spectrum at (22 757 $\pm$ 1) cm^{-1} represents the peak of highest energy (Fig. 2). It lies at the same energy as the dominating line of lowest energy in the excitation spectrum (Fig. 3). Therefore, this transition is classified as the electronic origin (0–0 line). It is assigned to the singlet–triplet transition ($S_0 \leftrightarrow T_1$), being mainly of LC $\pi\pi^*$ character, but because it is more strongly allowed compared to organic molecules some Rh4d mixing will also occur. This is displayed

by the fact that triplet excitation spectra are directly measurable for $[Rh(bpy)_3]^{3+}$ (see also Section 5 and Refs. [28–31,37–42].)

Obviously, the splitting of the triplet into three sublevels at zero magnetic field (ZFS) is not observable with the resolution obtained. However, using the method of optically deleted magnetic resonance (ODMR) spectroscopy it was possible to determine these splittings for different neat $[Rh(bpy\text{-}h_8)_3]X_3$ salts (with $X^- = Cl^-$, $(BF_4)^-$, $(ClO_4)^-$) [30,39–41]. The values for these salts deviate slightly. For example, for $[Rh(bpy\text{-}h_8)_3](ClO_4)_3$, Westra and Glasbeek [40,41] obtained splittings of 1.18 GHz ($2|E| \approx 0.04$ cm^{-1}), 2.32 GHz ($|D| - |E| \approx 0.077$ cm^{-1}), and 3.49 GHz ($|D| + |E| \approx 0.12$ cm^{-1}), respectively. These values lie in the same order as found for the uncoordinated bpy [46]. As expected, application of a magnetic field, e.g. $B = 12$ T, leads to a large splitting of the electronic origins, resulting in three resolvable components with a total splitting of 21 cm^{-1} (Fig. 2). These splittings correspond to $g \approx 1.9$, representing a typical value for spin triplets.

2.2.2. Decay properties and spin–lattice relaxation

In general, different triplet sublevels (exhibiting small splittings) are not in thermal equilibrium at $T = 1.3$ K, since relaxation processes between the sublevels (spin–lattice relaxation (SLR)) are largely frozen out at this temperature [14,47–49] (see also Section 4.3.1.) In this situation, the sublevels emit according to their individual occupation and decay properties. Indeed, for $[Rh(bpy\text{-}h_8)_3]^{3+}$ in $[Zn(bpy\text{-}h_8)_3](ClO_4)_2$ the emission is clearly multi-exponential and best fitted tri-exponentially with $\tau_I = (4.5 \pm 0.5)$ ms, $\tau_{II} = (1.35 \pm 0.1)$ ms, and $\tau_{III} = (0.65 \pm 0.05)$ ms ($T = 1.3$ K) (Fig. 3). Interestingly, microwave-induced rapid-passage experiments with neat $[Rh(bpy\text{-}h_8)_3](ClO_4)_3$ yielded lifetimes [41] that are not very different ($\tau_I = 6.7$ ms, $\tau_{II} = 4.6$ ms, and $\tau_{III} = 0.6$ ms; compare also to Ref. [39]). The deviations may be ascribed to the different matrices investigated. On increasing the temperature, the SLR becomes faster and finally results, near $T = 5$ K, in the thermal equilibrium of the three sublevels (see, for example, Refs. [23], [24], [47], [48] and [49]). This leads to a mono-exponential decay with an average decay time which can be expressed by the three low-temperature values, $\tau_{av} = 3(1/\tau_I + 1/\tau_{II} + 1/\tau_{III})^{-1}$ [47]. Using the values for $[Rh(bpy\text{-}h_8)_3]^{3+}$-doped $[Zn(bpy\text{-}h_8)_3](ClO_4)_2$, one obtains $\tau_{av} = (1.2 \pm 0.1)$ ms. Indeed, at $T = 5$ K the emission decays mono-exponentially with a decay time of (1.4 ± 0.1) ms, which is in agreement with the calculated τ_{av}. Similar behavior has also been observed for other transition metal complexes, such as $Pd(2\text{-}thpy)_2$ [22,24] (2-thpy$^-$: ortho-C-deprotonated 2-(2-thienyl)pyridine), and $Pt(qol)_2$ [50] (qol$^-$: 8-quinolinolate). In comparison, the emission decay components for the uncoordinated bpy are also given, measured [46] at $T = 1.2$ K (4 s, 0.77 s, 0.48 s) and at $T = 12$ K (0.82 s).

2.2.3. Vibrational and phonon satellite structures

The very rich structures, which occur as satellites in the emission and excitation spectra in addition to the electronic origins (Figs. 2 and 3), display a considerable amount of information about the properties of the involved electronic states. These satellites are assigned to transitions into vibrational levels of the ground state (emission) and of the lowest excited state(s) (excitation), respectively. Comparison

Table 1
Vibrational satellites (cm^{-1}) in the emission (at $T = 1.3$ K) of $[Rh(bpy\text{-}h_8)_3]^{3+}$ in $[Zn(bpy\text{-}h_8)_3](ClO_4)_2$ and of a $[Pt(bpy\text{-}h_8)_2]^{2+}$ trap in neat $[Pt(bpy\text{-}h_8)_2](ClO_4)_2$ compared to the Raman active modes

$[Rh(bpy\text{-}h_8)_3]^{3+}$		$[Pt(bpy\text{-}h_8)_2]^{2+}$		Assignments
Emission 0–0 ($T_1 \rightarrow S_0$): ($22\,757 \pm 1$) cm^{-1}	Raman[a]	Emission 0–0 ($T_1 \rightarrow S_0$): ($21\,237 \pm 1$) cm^{-1}	Raman[a]	
33		24		Lattice mode[b]
46		40		Lattice mode[b]
		55		Lattice mode[b]
62		64		Lattice mode[b]
82		79		Lattice mode[b]
119		121		
179		179		
		227	226	L mode[c]
278	279			L mode
377	382	381	382	L mode
421		417		M–L mode[d]
439		437		M–L mode[d]
452		471		M–L mode[d]
		726	727	FC[e], L mode
767	767	767	767	FC, L mode
800				767 + 33
829				767 + 62
849				767 + 82
1044	1048	1046	1045	FC, L mode
1178	1177	1178		L mode
1329	1327	1331	1332	FC, L mode
		1451		2 × 726
1507	1503	1502	1503	FC, L mode
1535		1535		2 × 767
1566	1570	1566	1566	FC, L mode
1609	1607	1611	1611	FC, L mode
1811		1813		767 + 1044/1046[f]
1945		1945		767 + 1178
2088		2088		2 × 1044/1046[f]
2274		2268		767 + 1507/1502[f]
2333		2333		767 + 1566
2376		2377		767 + 1609/1611[f]
3014		3000		2 × 1507/1502[f]
3132		3132		2 × 1566
3218		3221		2 × 1609/1611[f]

[a]Raman active vibrations. The spectra were measured at room temperature with neat $[Rh(bpy\text{-}h_8)_3](ClO_4)_3$ and $[Pt(bpy\text{-}h_8)_2](ClO_4)_2$, respectively.
[b]Lattice modes of $[Rh(bpy\text{-}h_8)_3]^{3+}$ in $[Zn(bpy)_3](ClO_4)_2$ are not correlated with those of $[Pt(bpy\text{-}h_8)_2]^{2+}(ClO_4)_2$.
[c]L: vibrational ligand mode.
[d]M–L: vibrational metal–ligand mode. The M–L modes of $[Rh(bpy\text{-}h_8)_3]^{3+}$ are not correlated with those of $[Pt(bpy\text{-}h_8)_2]^{2+}$.
[e]FC: progression-forming Franck–Condon mode.
[f]Fundamentals of $[Rh(bpy\text{-}h_8)_3]^{3+}$ and $[Pt(bpy\text{-}h_8)_2]^{2+}$, respectively.

of the vibrational energies of the ground state with Raman data shows very good agreement and thus consolidates the given assignments of the electronic origins (Table 1). The satellites, which appear in the low-energy range of the emission and excitation spectra up to about 100 cm^{-1} from the electronic origins, are assigned to lattice modes or to modes mixing with the low-energy vibrational modes of the complex (see, for examle, Ref. [24]). Several of these low-energy lattice modes are also found for $[Ru(bpy)_3]^{2+}$ (Section 4.3.1) and $[Os(bpy)_3]^{2+}$ [51] doped into the same $[Zn(bpy\text{-}h_8)_3](ClO_4)_2$ matrix.

Although a normal coordinate analysis is not yet available, a series of important assignments can still be given. The vibrational satellite structure is distinctly characterized by ligand modes, besides the phonon satellites and some extremely weak satellites of metal–ligand (M–L) character. These are determined from a comparison of the highly resolved spectra of $[Rh(bpy\text{-}h_8)_3]^{3+}$ with those of the partially deuterated Rh compounds [42]. The satellites of M–L character experience distinct energy shifts through the mass increase from $(bpy\text{-}h_8)$ to $(bpy\text{-}d_8)$. Thus, for $[Rh(bpy\text{-}h_8)_3]^{3+}$ the 421, 439, and 452 cm^{-1} modes are identified as M–L modes (Table 1 and Section 3.2). It is emphasized that the very weak intensities of M–L satellites display a very weak metal contribution to the wavefunctions of the involved electronic states [21,26,27].

It is interesting that the vibrational satellites do not show any dominating vibrational Franck–Condon progression, as might be deduced from the less well-resolved spectra published previously. However, the emission spectra reveal that for some prominent vibrational modes, the 0–1 and also the 0–2 members of weak progressions are found (e.g. for the 767, 1044, 1507, 1566, and 1609 cm^{-1} fundamentals) [42] (see also Fig. 2 and Table 1). The intensity distributions of these weak progressions may be applied to determine the corresponding Huang–Rhys factors S, using the expression $S = v(I_v/I_{v-1})$, where I_v is the intensity of one member of a specific progression and v is its vibrational quantum number [16,52,53]. S is directly related to the Franck–Condon factor of the respective vibrational mode, and increases with an increase in the size of the shift of the nuclear equilibrium positions of the potential hypersurfaces between the ground and excited states for the specific vibrational mode. These progression-forming Franck–Condon modes are totally symmetric. For all progressions observed for $[Rh(bpy)_3]^{3+}$, one obtains $S \leq S_{max} \approx 0.3$. The corresponding modes are characterized by FC in Table 1. Presumably, all other stronger satellites appearing in Fig. 2 also represent FC modes which, however, exhibit smaller S values. Nearly the same value of 0.3 has also been found for uncoordinated bpy [27,54]. Compared with the known range of S values observed for other compounds—values of up to ten have been reported (see, for example, Refs. [52], [53], [55] and [56])—it follows that a maximum value of 0.3 of the Huang–Rhys factor must be regarded as very small. This implies that the nuclear equilibrium positions of the triplet state and the ground state are similar for $[Rh(bpy\text{-}h_8)_3]^{3+}$.

All prominent vibrational satellites are accompanied by phonon satellites. For example, combinations of the 767 cm^{-1} mode with the 33, 62, 82 cm^{-1} lattice modes are clearly discernible for $[Rh(bpy\text{-}h_8)_3]^{3+}$ (Fig. 2, Table 1). However, in most cases these phonon satellites are smeared out to bands. These bands are in part responsible

for the unresolved background observed in the emission and excitation spectra. In particular, unusual structures are found when several vibrational satellites with their respective phonon side bands overlap (for example, see the range of 1507, 1566 and 1609 cm^{-1} peaks in Fig. 2). In low-resolution spectra, such a structure will appear as one dominating peak and might be taken as one member of a fictitious progression (see, for example, Fig. 1 and the examples given in Refs. [22] and [57]). Further, all clearly discernible peaks in the emission spectra at energies larger than about 1650 cm^{-1} are assigned to combinations of prominent vibrational modes or to members of very weak Franck–Condon progressions (Table 1). The occurrence of combinations with weak intensities in the vibrational satellite structures indicates small shifts along different normal coordinates (see, for example, Ref. [56]).

A comparison of the excitation (Fig. 3) with the emission (Fig. 2) spectra allows analysis of the changes in vibrational energies or (indirectly) force constants due to an excitation of T_1. For this comparison, modes have to be identified which correspond to each other. Since normal coordinate analyses of ground and excited states are not available, the information provided by the structures and intensity distributions of the spectra can only be used to specify a series of correlated vibrations. Such a procedure is further justified if the obtained correlation also fits for the equivalent mode of the related per-deuterated complex. For example, it is found that the energies of the 179, 767, and 1044 cm^{-1} ground state modes of $[Rh(bpy\text{-}h_8)_3]^{3+}$ are shifted to 174, 727, and 1013 cm^{-1} of T_1, respectively [42]. Such an energy reduction is not unexpected for $\pi\pi^*$ transitions, where the force constants should decrease.

2.3. Lowest triplets in $[Rh(bpy\text{-}h_8)_2(bpy\text{-}d_8)]^{3+}$ and $[Rh(bpy\text{-}d_8)_3]^{3+}$

Highly resolved emission and excitation spectra of partially and per-deuterated Rh complexes doped into $[Zn(bpy\text{-}h_8)_3](ClO_4)_2$ were reported in Ref. [42], in which a series of specific properties was deduced which are also important in the context of this review. The lowest excited triplet of $[Rh(bpy\text{-}d_8)_3]^{3+}$ lies at $(22\,818 \pm 1)$ cm^{-1}. Thus, per-deuteration of the complex leads to a blue shift of the electronic origin of (61 ± 1) cm^{-1}. This occurrence of a blue shift shows that on average the vibrational force constants in the excited state are smaller than those of the electronic ground state (see Section 2.2.3. and Ref. [57]). For the uncoordinated bpy, one finds (in an *n*-heptane Shpol'skii matrix) a deuteration-induced blue shift of about 86 cm^{-1} [54]. A comparison of these two values indicates that an excitation of T_1 of the complex induces slightly smaller changes of force constants than in the uncoordinated ligand.

The vibrational satellite structure of $[Rh(bpy\text{-}d_8)_3]^{3+}$ exhibits drastic changes with respect to $[Rh(bpy\text{-}h_8)_3]^{3+}$, since the emission from the deuterated ligands shows all the effects which are usually observed on deuteration of the emitting centers [21,51,57–61] In particular, (i) all the vibrational energies (except phonons) are red shifted, (ii) the intensity distribution of the vibrational satellite structure is partly changed owing to alterations of the forms (PEDs) of the normal coordinates [60], (iii) the long component of the emission decay increases from 4.5 to 13.6 ms owing

to a reduction in non-radiative deactivation processes, and (iv) the electronic transition energy is blue shifted, as discussed above.

The *excitation* spectrum of $[Rh(bpy\text{-}h_8)_2(bpy\text{-}d_8)]^{3+}$ shows *two* dominating lines at $(22\,757 \pm 1)\ cm^{-1}$ and $(22\,818 \pm 1)\ cm^{-1}$ with an intensity ratio of 2:1 [42]. These lines lie at the same energies as the electronic origins of the per-protonated and per-deuterated compounds. Therefore, these two transitions are assigned to electronic origins of the protonated and deuterated ligands, respectively. Apparently, the energy of the electronic origin of a specific (coordinated) ligand does not depend on the other ligands. This is consistent with the assignment of these transitions as ligand centered, exhibiting only a very small degree of ligand–ligand coupling. Moreover, this is displayed in the vibrational satellite structure of the excitation spectrum of $[Rh(bpy\text{-}h_8)_2(bpy\text{-}d_8)]^{3+}$, since it may be interpreted as resulting from superimposed spectra of per-deuterated and per-protonated compounds, weightened by the number of ligands.

Interestingly, the emission of $[Rh(bpy\text{-}h_8)_2(bpy\text{-}d_8)]^{3+}$ displays totally different behavior. It is definitely ascribed to the protonated ligand(s), since the spectra of the per-protonated and partially deuterated compounds are nearly identical (the only exception being some shifts of the very weak vibrational M–L satellites). The same emission spectrum is found, even when the deuterated ligand at $22\,818\ cm^{-1}$ or any other higher-lying state is excited. Clearly, efficient intramolecular energy transfer occurs from the deuterated ligand to the protonated ligand(s) (see Section 2.4).

A further interesting aspect is that from the absence of even dominating satellites corresponding to high-energy ligand modes of $(bpy\text{-}d_8)$ in the emission spectrum of the partially deuterated Rh compound [42], it can be concluded that for high-energy internal-ligand vibrations remarkable coupling through space or via the metal may be disregarded (see also Section 4.3.2).

2.4. Dual emission versus intramolecular energy transfer

As discussed in Section 2.3, $[Rh(bpy\text{-}h_8)_2(bpy\text{-}d_8)]^{3+}$ emits only from the protonated ligand, even if the deuterated one is excited selectively. Apparently, the rate $P_{D\text{-}A}$ of energy transfer from the deuterated ligand (donor D) to the protonated ligand (acceptor A) is much larger than the decay rate τ_{III}^{-1} of the fast decaying sublevel of the deuterated ligand. Thus, $P_{D\text{-}A} \gg \tau_{III}^{-1} \approx 1.7 \times 10^3\ s^{-1}$ (from Ref. [42]). This value, providing a lower limit, is extremely small for a resonant energy transfer, and the effective rate is presumably several orders of magnitude larger. However, this estimate shows that even a very low transfer rate will quench the donor emission. Thus, the occurrence of "dual emission" is prevented. Similar or related considerations have been applied to other heteroleptic complexes, for example to $[Rh(bpy)_n(phen)_{3-n}]^{3+}$ ($n=1$, 2; phen=1,10-phenanthroline) [62], $[Ir(bpy)_n(phen)_{3-n}]^{3+}$ ($n=1$, 2) [63], $[Ir(bpy)(phpy)_2]^{3+}$ (phpy=2-phenylpyridine) [62,64], and to $[Pt(bpy\text{-}h_8)(bpy\text{-}d_8)]^{2+}$ (see Section 3.2). In these cases "dual emission" could always be excluded. However, several authors have reported the occurrence of such a "dual emission", e.g. for $[Rh(bpy)_n(phen)_{3-n}]^{3+}$ dissolved in glass-

forming matrices [28,31,37,38]. However, this observed behavior may be interpreted alternatively, as has been discussed by Henderson and Imbusch [53] for a related situation and by Güdel and co-workers [62] for the above-mentioned complexes. According to these considerations, the "dual emission" could result from superpositions of the spectra resulting from the same chromophores which, however, occupy different types of sites in the matrices investigated. For example, $[Rh(bpy)_n(phen)_{3-n}]^{3+}$ may lie in one specific site, where the LC $\pi\pi^*$ transitions of the phen ligands are energetically stabilized, while for other sites (other environments) the transitions of the bpy ligands are lower in energy. In such a situation, it might be difficult to interpret the measured spectra correctly, if they are not sufficiently resolved.

3. $[Pt(bpy)_2]^{2+}$

Planar platinum complexes have the tendency to form linear stacks in the solid state. Typical examples are $[Pt(CN)_4]^{2-}$ [65,66] and a series of heteroleptic Pt(II)–α-diimine complexes [67,68] (see also Ref. [69]). However, the effects of solid state interactions are not the subject of the present investigation.

Fig. 4 is reproduced to give an introduction to the absorption and emission spectra of dissolved $[Pt(bpy)_2]^{2+}$. These spectra correspond largely to those published elsewhere [68,70–72]. A comparison with the spectra of $[Rh(bpy)_3]^{3+}$ (Fig. 1) shows that both compounds have a similar absorption and the transitions observed may similarly be assigned to singlet–singlet transitions of $\pi\pi^*$ character (compare Refs. [68] and [71]). The additional peak in the absorption of $[Pt(bpy)_2]^{2+}$ might be assignable to ^{1}MLCT transitions according to the energy ($\approx$28 000 cm^{-1}), $\epsilon \approx 2\text{–}3 \times 10^3$ l mol^{-1} cm^{-1}, and general considerations with respect to oxidation and reduction potentials [73]. The emitting state is assigned as a triplet (relatively

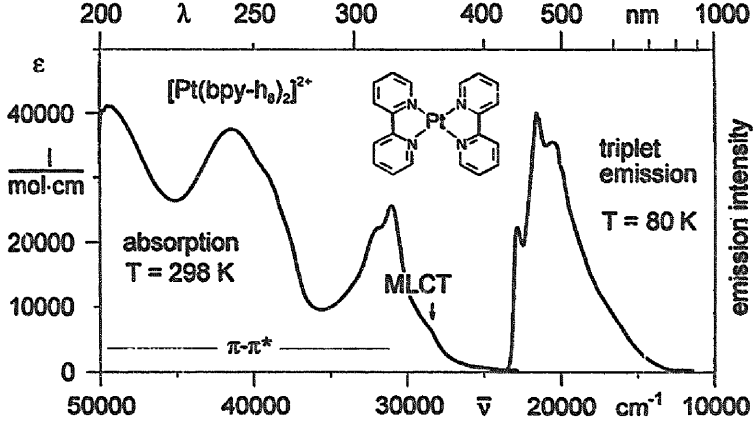

Fig. 4. Ordinary absorption and emission spectra of $[Pt(bpy)_2]^{2+}$ dissolved in DMF (λ_{exc} = 320 nm).

long lifetime) [71], but its electronic parentage has only very prudently been proposed as being of LC $\pi\pi^*$ character [68,71,74]. In this contribution, it will be shown that this assignment is largely correct, although a small MLCT admixture is effective (see Section 3.2 and Section 5).

3.1. $[Pt(bpy)_2]^{2+}$ in a crystalline $[Pt(bpy)_2](ClO_4)_2$ matrix

As outlined in Section 2.1, it is important to find an adequate matrix, if highly resolved spectra of a specific chromophore have to be registered. Hitherto, an inert matrix which fulfills all the required conditions could not be found. However, in $[Pt(bpy)_2](ClO_4)_2$ single crystals defined $[Pt(bpy)_2]^{2+}$ traps are found, whose triplets are several cm^{-1} below those of the majority of complexes or below the triplet exciton band. Thus, by exciting these traps selectively via an exactly tuned dye laser, the desired spectrum is obtained. An important additional condition is that the sample temperature is low enough to prevent energy migration versus thermally populated energetically higher lying traps (compare with Fig. 5). This procedure is successful for $[Pt(bpy)_2](ClO_4)_2$. However, the disadvantage of a relatively small free spectral range of about 40 cm^{-1} has to be accepted for the excitation spectra. Moreover, the symmetry of the spectroscopically selected trap is not known.

3.2. Characterization of the lowest triplet of $[Pt(bpy)_2]^{2+}$

Fig. 5a reproduces the 4.2 K emission spectrum of $[Pt(bpy\text{-}h_8)_2]^{2+}$ [75]. A comparison of this spectrum with that of $[Rh(bpy\text{-}h_8)_3]^{3+}$ (Fig. 2) shows both to be nearly

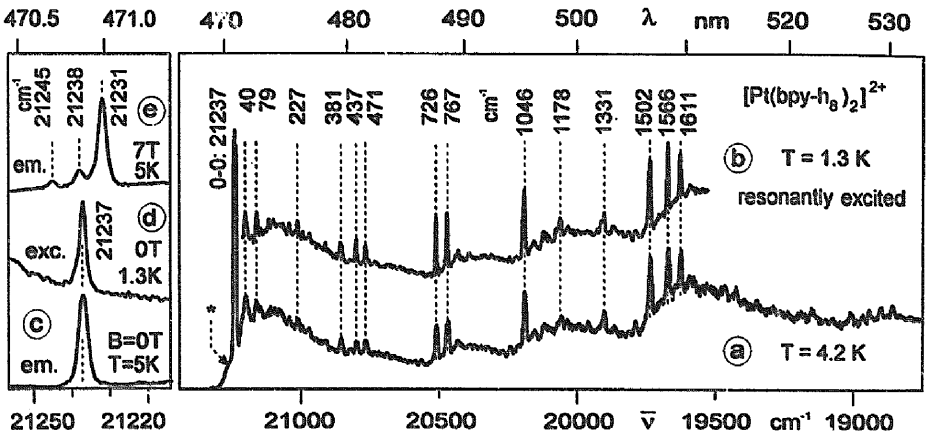

Fig. 5. Highly resolved emission of a $[Pt(bpy\text{-}h_8)_2]^{2+}$ trap in neat $[Pt(bpy\text{-}h_8)_2](ClO_4)_2$ (see Ref. [75]). (a) Excitation energy $\tilde{\nu}_{exc}=21\,839$ cm^{-1} ($\triangleq$457.9 nm). The asterisk characterizes an emission from higher-lying trap(s). (b) Resonantly excited emission ($\tilde{\nu}_{exc}=21\,237$ cm^{-1}, electronic origin $S_0 \rightarrow {}^3\Gamma_1$). (c)–(e) Region of the electronic origin(s) on an enlarged scale. The excitation (d) is detected at 19 626 cm^{-1} ($\triangleq$1611 cm^{-1} satellite). The crystals were grown from DMF.

identical (see also Table 1). Therefore, most arguments developed in Section 2.2 for $[Rh(bpy)_3]^{3+}$ also hold for $[Pt(bpy)_2]^{2+}$.

The electronic origin of the $S_0 \leftrightarrow T_1$ transition for the trap investigated lies at $(21\,237 \pm 1)$ cm^{-1} in emission (Fig. 5c) and excitation (Fig. 5d). T_1 should exhibit a ZFS, but this is not resolvable in the registered spectra. Moreover, no direct evidence of T_1 splitting by ODMR or other measurements applying microwave techniques has yet been given. However, at $T = 1.3$ K the triplet sublevels display their individual properties by showing three different decay times (Fig. 6, inset). Furthermore, the triplet splits into three components, when a high magnetic field of $B = 7$ T is applied (Fig. 5e). The total splitting of ≈ 14 cm^{-1} corresponds to a g-value of about two.

The electronic origin corresponding to T_1 of $[Pt(bpy\text{-}h_8)_2]^{2+}$ lies about 1500 cm^{-1} lower in energy than that of $[Rh(bpy\text{-}h_8)_3]^{3+}$. Such a shift seems to be somewhat too large to be ascribed to a matrix effect. Presumably, this red shift may be attributed, at least to some small extent, to a small MLCT admixture with the lowest triplet of $[Pt(bpy\text{-}h_8)_2]^{2+}$. This is supported by the much shorter emission decay times of $[Pt(bpy\text{-}h_8)_2]^{2+}$ and by the intensity distribution of the vibrational satellite structure in the energy range of M–L modes. The emission of $[Pt(bpy\text{-}h_8)_2]^{2+}$ exhibits a more pronounced intensity of M–L vibrational satellites than the emission of $[Rh(bpy\text{-}h_8)_3]^{3+}$. These intensities represent (for the bpy compounds investigated) a measure of an admixture of MLCT or metal-d character with the electronic wavefunctions involved [21,27] (compare Fig. 2 to Fig. 5a). The M–L modes of $[Pt(bpy\text{-}h_8)_2]^{2+}$, lying at 417, 437, and 471 cm^{-1}, are identified by

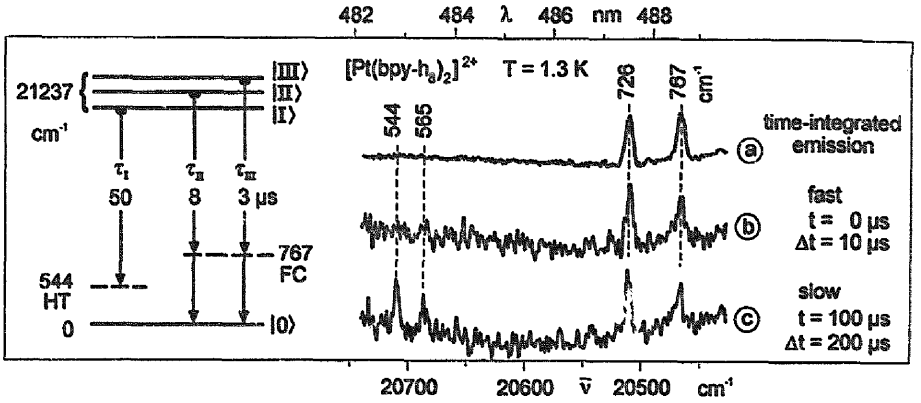

Fig. 6. Time-resolved and time-integrated emission of a $[Pt(bpy\text{-}h_8)_2]^{2+}$ trap in neat $[Pt(bpy\text{-}h_8)_2](ClO_4)_2$ in the region of the vibrational satellite structure (see Ref. [75]) (a) The time-integrated spectrum is line narrowed (resonantly excited at $\bar{\nu}_{exc} = 21\,237$ cm^{-1}; electronic origin $S_0 \rightarrow T_1$). (b, c) The time-resolved spectra are excited at $\bar{\nu}_{exc} = 22\,075$ cm^{-1} ($\triangleq 453$ nm). For further data see Fig. 5. Inset: energy level scheme for the triplet sublevels and the corresponding decay times for $T = 1.3$ K. The radiative deactivation from $|I\rangle$ is, at least in part, vibronically induced by Herzberg–Teller (HT) modes, while the deactivation from $|II\rangle$, $|III\rangle$ to the ground state $|0\rangle$ is induced by spin–orbit coupling and accompanied by Franck–Condon modes.

their energy shifts compared to the satellites of $[Pt(bpy\text{-}h_8)(bpy\text{-}d_8)]^{2+}$, while the energies of the ligand modes remain unshifted (see also Section 2.2.3 and Table 1).

According to the fact that the three triplet sublevels emit independently at $T=$ 1.3 K, the usually registered emission spectrum is expected to consist of a superposition of three different spectra. The long-lived triplet sublevel (called $|I\rangle$ in Fig. 6, inset) corresponds to a largely forbidden transition at the electronic origin $|0\rangle \leftrightarrow |I\rangle$, but Herzberg–Teller (HT) vibrational modes are expected to open radiative deactivation paths. This effect should be displayed by specific vibrational satellites [23,25,76,77]. However, the fast-decaying sublevels $|II\rangle$ and $|III\rangle$ carry more allowedness (mainly owing to spin–orbit coupling; for detailed arguments see Refs. [23] and [25]), and thus the main radiative deactivation will occur via the electronic origins and by vibrational Franck–Condon (FC) satellites. The resolution of the spectra measured is not sufficient to resolve these effects *spectrally*, since the ZFS of the electronic origins is expected to be only of the order of 0.1 cm^{-1}. However, *time-resolved* emission spectra should display the different properties, at least of $|I\rangle$ compared to $|II\rangle$ and $|III\rangle$, owing to the large differences in the individual decay times. Indeed, this effect is observed for $[Pt(bpy\text{-}h_8)_2]^{2+}$ over a small spectral range of the total emission (Fig. 6). These results show in particular that the 544 and 565 cm^{-1} satellites, occurring in the slow spectrum (Fig. 6c), deactivate the emission from state $|I\rangle$. While, for example, the 767 cm^{-1} mode is less selective and presumably belongs to all three deactivation paths. Thus, specific time-resolved vibrational satellites directly display properties of the individual sublevels, which cannot be resolved by conventional optical spectroscopy.

The behavior described is already well known for organic molecules [76,77], but has only very recently been observed for a series of transition metal complexes, e.g. $Pd(2\text{-}thpy)_2$ [23], $Pt(2\text{-}thpy)_2$ [25], $[Ru(bpy)_3]^{2+}$ (Ref. [78] and Section 4.3.1), and $[Rh(bpy)_3]^{3+}$ [42,79]. This behavior may be regarded as a rather general phenomenon. Recently, highly resolved emission spectra of $[Pt(bpy\text{-}h_8)(bpy\text{-}d_8)]^{2+}$ have also been obtained [75]. These are nearly identical to the spectra of the per-protonated compound, with the exception of some spectral shifts in the range of the M–L and lattice modes (different host). Thus, "dual emission" can also be excluded for partially deuterated $[Pt(bpy)_2]^{2+}$ (see also Section 2.4).

4. $[Ru(bpy)_3]^{2+}$

$[Ru(bpy)_3]^{2+}$ is a complex which is still of considerable interest, although a large number of investigations have already been carried out (see, for example, reviews [4,5,12,18–20,78,80–87]). In this report, we want to focus the attention on the electronic and vibronic properties of the lowest excited states. It is intended to base the following discussion mainly on highly resolved emission and excitation spectra, as well as on interesting effects observed by time-resolved emission measurements. However, before details are discussed, it is suitable to show Fig. 7 for an introduction to the room temperature absorption and 80 K emission spectra. These correspond largely to the spectra published elsewhere (see, for example, Ref. [4]). The spectral

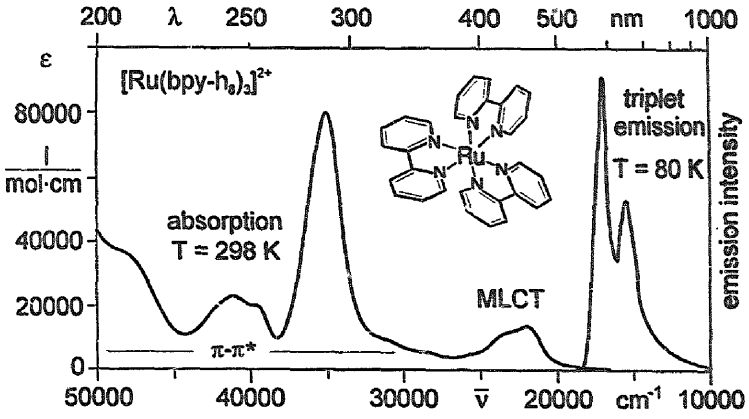

Fig. 7. Ordinary absorption and emission of $[Ru(bpy)_3]^{2+}$ dissolved in water (λ_{exc}=440 nm).

features above about 33 000 cm^{-1} are usually assigned to singlet–singlet transitions of $\pi\pi^*$ character. These strong transitions lead to "exciton coupling", even when d-contributions are neglected, as discussed for $[Rh(bpy)_3]^{3+}$ (Section 2 and Refs. [32], [33], [34], [35] and [36]). As a consequence, the corresponding excited singlet states have to be assigned to the whole ligand system. A localization can only occur under specific conditions, which are discussed in Section 4.2 and Refs. [78,85]. In the literature, the absorption structure near 22 000 cm^{-1} is, in general agreement, assigned to result from Ru4d-bpyπ^* ^{1}MLCT transitions, the ground state being a singlet [4,5,12,18–20,78,80–95]. While, the emission at 80 K stems—also in general agreement—from a series of ^{3}MLCT states [18,21,28,82,83,95]. At 300 K, one can additionally detect a weak component of a singlet emission ($^1A_2$ in D_3) [96–99]. A more detailed discussion on the basis of the broad spectrum shown in Fig. 7 does not seem to be very successful.

4.1. $[Ru(bpy)_3]^{2+}$ aggregates in $[Zn(bpy)_3](ClO_4)_2$

$[Zn(bpy)_3](ClO_4)_2$ represents an inert matrix with respect to the energy range of the MLCT transitions of $[Ru(bpy)_3]^{2+}$. In particular, it is possible to obtain highly resolved spectra (with halfwidths of less than 3 cm^{-1}) for the lowest ^{3}MLCT transitions [57,85,100]. This indicates that the inhomogeneous broadening effects and/or the electron–phonon coupling strengths are even somewhat smaller than those found for a series of other matrices, for which fine structures had already been reported more than a decade ago [101–104]. Thus, the $[Zn(bpy)_3](ClO_4)_2$ matrix seems to be very promising for detailed studies if, for example, the techniques of luminescence and excitation line narrowing are applied. However, the distribution of the $[Ru(bpy)_3]^{2+}$ guest molecules in this host material causes several problems. This can already be seen by inspecting doped crystals. Their central parts are always deeply red colored while the outer regions are nearly transparent. Moreover, the crystals may exhibit a number of red spots. This phenomenon occurs even

when crystals are grown from very low-concentration solutions (e.g. $[Ru(bpy)_3]^{2+}/[Zn(bpy)_3]^{2+} < 0.03\%$). Thus, the tendency of $[Ru(bpy)_3]^{2+}$ to form aggregates is highly pronounced for this guest–host system. Such behavior is not unusual (see, for example, Ref. [105]). It corresponds to an effective distribution coefficient (segregation coefficient) k_{eff} significantly larger than unity, e.g. values of $k_{eff} \approx 5$ for the compounds studied have been found. (k_{eff} is the ratio of the guest concentration in the matrix relative to its concentration in solution.) The fact that k_{eff} deviates significantly from unity is already expected from a comparison of the structures of $[Zn(bpy)_3](ClO_4)_2$ [106,107] and $[Ru(bpy)_3](ClO_4)_2$ [106,108]. Although their space groups are identical, the cell parameters deviate significantly. This implies that the compounds exhibit different intermolecular interactions. For further details see Ref. [85].

The situation for $[Ru(bpy\text{-}d_8)_3]^{2+}$ and $[Ru(bpy\text{-}h_8)_2(bpy\text{-}d_8)]^{2+}$ in $[Zn(bpy\text{-}h_8)_3](ClO_4)_2$ is similar with respect to the non-uniform colors of the doped crystals, again corresponding to $k_{eff} > 1$. Up to now, the crystal structures of the deuterated Ru compounds are not available, and thus it is not even known whether the deuterated compounds and the $[Zn(bpy\text{-}h_8)_3](ClO_4)_2$ matrix have the same space groups.

In summary, $[Zn(bpy)_3](ClO_4)_2$ represents a suitable matrix for different $[Ru(bpy)_3]^{2+}$ chromophores, but the dopants are not statistically distributed in the $[Zn(bpy)_3](ClO_4)_2$ host. Nearest-neighbor interactions and effects caused by the formation of aggregates have to be taken into account. Moreover, much care should be taken with detailed assumptions, for example, about the symmetries of the doped complexes, since the individual host–guest interactions are not known. In particular, the situation is even more complicated for low-symmetry dopants such as the partially deuterated $[Ru(bpy)_3]^{2+}$ complexes.

4.2. Localization/delocalization

The properties of the lowest excited (triplet) states of $[Ru(bpy)_3]^{2+}$ or of related tris-chelates are often discussed in a localized model, where only one of the three ligands and the metal are involved. In the literature, there are currently two, mutually excluding localization models, and also—in contradiction to both of these—a description based on delocalization. Thus, some basic ideas concerning the physical implications related to the process of localization or its exclusion will be discussed here [78,109]. For further details see Ref. [85].

4.2.1. Small interaction energy and localization by a weak distortion

Firstly, it is appropriate to discuss the situation of LC triplets of $\pi\pi^*$ character and assume the existence of a weak ligand–ligand interaction, even when the coupling via the metal is unimportant. If the different ligands are symmetry related (e.g. by a C_2 operation), the excited state wavefunctions can be described by symmetry-adapted linear combinations of the wavefunctions of the individual ligands. The resulting wavefunctions correspond to a delocalized description [110]. In particular, one of the resulting electronic states of the coupled system is stabilized energetically

by an energy represented by B. With the assumed weak ligand–ligand coupling B is expected to be of the order of only a few cm^{-1}, similar to triplet exciton band widths in organic solid state compounds [33,111–114] (see also the discussion in Ref. [104].) In a second step, the effect of the transition metal is introduced by allowing an additional weak admixture of $^3dd^*$ or ^{3}MLCT states to the $^3\pi\pi^*$ states, as well as weak spin–orbit coupling (see Section 5). This will certainly lead to an increase in the effective ligand–ligand interaction and to a slight increase in the electronic stabilization energy B. However, environment-induced interactions (distortions), which may be different for individual ligands of the same complex (inhomogeneity effects), can easily remove the equivalence of the ligands and lead to individual energy shifts significantly larger than the electronic stabilization energy B. As a consequence, even a weak distortion may decouple the different ligands, and the electronic states will be localized onto the individual ligands. This type of localization by a *weak distortion* seems to describe the situation of $[Rh(bpy)_3]^{3+}$ well, since the excitation may be regarded as belonging to one specific bpy ligand [40]. Moreover, $[Rh(bpy\text{-}h_8)_2(bpy\text{-}d_8)]^{3+}$ exhibits an additional "chemically-induced" distortion, which decouples the (bpy-d_8) ligand from the (bpy-h_8) ligand even further.

4.2.2. Large interaction energy and localization by a strong distortion

It is obvious that the simple model discussed above, regarding the ligands as separate molecular units, will no longer be applicable if the electronic orbitals of the metal and ligands strongly overlap, as for ^{3}MLCT states. In this distinctly covalent situation, determination of the the energy states of the complex requires more sophisticated procedures than discussed above. However, without any doubts, it can be concluded (for example, by applying the Heisenberg uncertainty principle) that increasing overlap leads to spatial extension (delocalization) of the electronic wavefunctions. This will result in a significantly larger stabilization energy B than for non-overlapping molecular subunits [110]. A calculation of B for $[Ru(bpy)_3]^{2+}$ has not yet been carried out, but a first estimate of a lower limit leads to a value of B in the order of 10^3 cm^{-1}, as can be deduced from Refs. [89,90,92,93]. These considerations show that electronic delocalization stabilizes the lowest excited states. This is a well-accepted phenomenon, which is similarly valid for conjugated organic molecules (see, for example, Ref. [110]). Nevertheless, localization can still occur if an intramolecular or environmentally-induced distortion leads to an energy stabilization of $E_L > B$. Such a large value of $E_L \approx 10^3$ cm^{-1} can only be effected by a relatively *strong distortion*. (For a more detailed discussion of this aspect see Refs. [78,85,109].) Obviously, this type of localization will result in a series of pronounced spectroscopic features. For example, compared to the delocalized situation, one would expect to find (i) distinct changes of vibrational energies in these localized and distorted excited states (see Refs. [115,116,117] for dissolved complexes and the critical remarks in Ref. [51] as well as the detailed discussion in Ref. [85]), (ii) a significant increase of the blue shifts of the electronic transitions on deuteration (see Ref. [57]), (iii) Franck–Condon progressions becoming dominant in the emission and absorption spectra (see Section 4.3.1. and Refs. [57,78]), and (iv) very character-

istic vibrational satellite structures in the emission and excitation spectra of partially deuterated complexes (Section 4.3 and Refs. [21] and [51]). None of these effects can be observed with $[Ru(bpy)_3]^{3+}$ or $[Os(bpy)_3]^{2+}$ in rigid matrices for their three lowest excited states [21,51,57,78,85]. Therefore, localization due to a strong distortion can be excluded for these complexes doped into $[Zn(bpy)_3](ClO_4)_2$.

The situation is possibly different at room temperature, when the complexes are dissolved in fluid and polar solutions [115–117]. Polar solvent molecules may lead to an unsymmetric distortion by a strong complex–solvent interaction, as proposed earlier in Ref. [97] (see also Refs. [51] and [83]). This might lead to an energy stabilization $E_L > B$. (Obviously, stabilization can easily be obtained by the chemical substitution of one ligand.) However, a discussion of the whole system, the metal complex and its non-rigid solvent cage is beyond the scope of this contribution.

In recent investigations, Riesen and co-workers [118–120] proposed that for $[Ru(bpy)_3]^{2+}$ localization can even occur from a weak distortion, even in rigid matrices and at low temperatures, similar to the situation described for $[Rh(bpy)_3]^{3+}$ (see above). In particular, these authors assume that the ^{3}MLCT states in $[Ru(bpy)_3]^{2+}$ are largely isolated onto different (Ru-bpy) subunits of the same complex. They claim that the interaction energy between a ^{3}MLCT state of one (Ru-bpy) subunit and an identical state of a symmetry-related (C_2 operation) second (Ru-bpy) subunit of the same $[Ru(bpy)_3]^{2+}$ complex is less than 0.1 cm^{-1} [118]. Thus, a very weak environment-induced distortion will—according to that model—lead to localization. However, an assumed interaction energy of less than 0.1 cm^{-1} is more than four orders of magnitude(!) smaller than estimated according to the current literature [21,89,90,92,93,78] for B of $[Ru(bpy)_3]^{2+}$. This value is even about one order of magnitude smaller than expected for ligand-centered $^3\pi\pi^*$ states in $[Rh(bpy)_3]^{3+}$. The authors [118,119] do not give any physical reason for their unusually and unexpectedly small value of the interaction energy of less than 0.1 cm^{-1}. However, it will be shown in Section 4.3.2 and Section 4.3.3 that spectroscopic features, which have been ascribed in Refs. [118,119] to the different (Ru-bpy) subunits of the artificially cut complex, may be related to different neighboring $[Ru(bpy)_3]^{2+}$ complexes in the matrix. Such neighbor arrangements occur even at very low nominal concentrations, owing to the specific tendency to aggregate as observed for $[Ru(bpy)_3]^{2+}$ in $[Zn(bpy)_3](ClO_4)_2$ (see Section 4.1). This important property was not taken into account in Refs. [118] and [119].

4.3. Characterization of the lowest ^{3}MLCT states of $[Ru(bpy)_3]^{2+}$

Highly resolved emission and excitation spectra of $[Ru(bpy)_3]^{2+}$ have so far only been reported by Yersin and co-workers (see, for example, Refs. [12,21,57,83,98,101–104]), Krausz and co-workers (see, for example, Refs. [82,84,118–122]), and Hirota and co-workers (see, for example, Refs. [100,123]). Three low-lying electronic states of $[Ru(bpy)_3]^{2+}$ of ^{3}MLCT character were clearly identified, called $|I\rangle$, $|II\rangle$, and $|III\rangle$; $|0\rangle$ being the ground state (Fig. 8). This assignment is out of the question, even when problems resulting from aggregation (Section 4.1) and energy transfer within the aggregates are taken into account, since

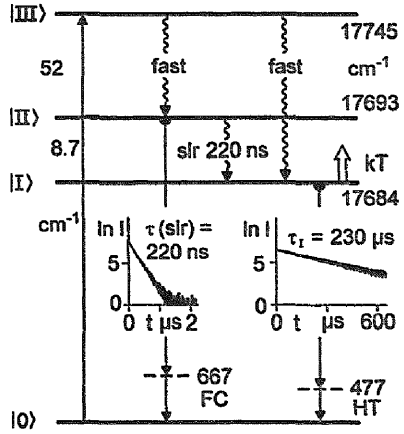

Fig. 8. Energy level diagram for the three lowest excited states of $[Ru(bpy\text{-}h_8)_3]^{2+}$ in $[Zn(bpy\text{-}h_8)_3](ClO_4)_2$. The spin–lattice relaxation (SLR) from states $|II\rangle$ to $|I\rangle$ is hindered at $T=1.2$ K, owing to a slow process of direct phonon emission resulting in a decay time of 220 ns [78,85,132]. The emission from $|II\rangle$ is governed by Franck–Condon (FC) active modes, while the emission from $|I\rangle$ also shows Herzberg–Teller (HT) activity. State $|I\rangle$ emits with its usual emission lifetime of $\tau_I=230$ µs. The energy level schemes of $[Ru(bpy\text{-}h_8)_2(bpy\text{-}d_8)]^{2+}$ and $[Ru(bpy\text{-}d_8)_3]^{2+}$ are very similar. The electronic origins (same matrix) lie at 17 684 cm^{-1} (I), 17 693 cm^{-1} (II), and 17 745 cm^{-1} (III) (lowest site A [21] of the partially deuterated compound); and at 17 724 cm^{-1} (I), 17 733 cm^{-1} (II), and 17 787 cm^{-1} (III) (per-deuterated compound).

these effects reveal themselves, especially by specific features within the inhomogeneous linewidths (Section 4.3.2). In particular, in a high-symmetry [124] matrix such as $[Ru(bpy)_3](PF_6)_2$, these states can be assigned to degenerate representations. This is, however, still under debate; compare Refs. [83,93,98,103,125,126] with Refs. [118–122,127].

The energies of the three electronic states depend slightly on the matrix investigated. Matrix-induced shifts of about 200 cm^{-1} are found (see, for example, Refs. [83,85]). These are approximately similar for all three states, which indicates that they have the same orbital parentage. Therefore, they may be assigned as sublevels of one ^{3}MLCT state [27]. This is further supported by the facts that under high pressure, the three states exhibit—within ± 0.7 cm^{-1} $kbar^{-1}$—the same red shifts of 13 cm^{-1} $kbar^{-1}$ (at $T=1.7$ K) [128], and that they show a Zeeman interaction under high magnetic fields [122,126]. Further properties of these three states and interesting new physical implications are discussed below.

4.3.1. Spin–lattice relaxation and time-resolved emission of $[Ru(bpy\text{-}h_8)_3]^{2+}$

Fig. 9a shows the usual, time-integrated low-temperature emission of $[Ru(bpy\text{-}h_8)_3]^{2+}$-doped $[Zn(bpy\text{-}h_8)_3](ClO_4)_2$ with a dominant line I at $(17\,684\pm 1)$ cm^{-1}. A corresponding excitation line is not observed (Fig. 9b). Nevertheless, this transition may clearly be assigned as the electronic origin $|I\rangle\rightarrow|0\rangle$, which exhibits an extremely weak transition probability. (Detailed arguments for this assignment are given in Refs. [21,57,83,85]). In addition to this dominating line I, resolved

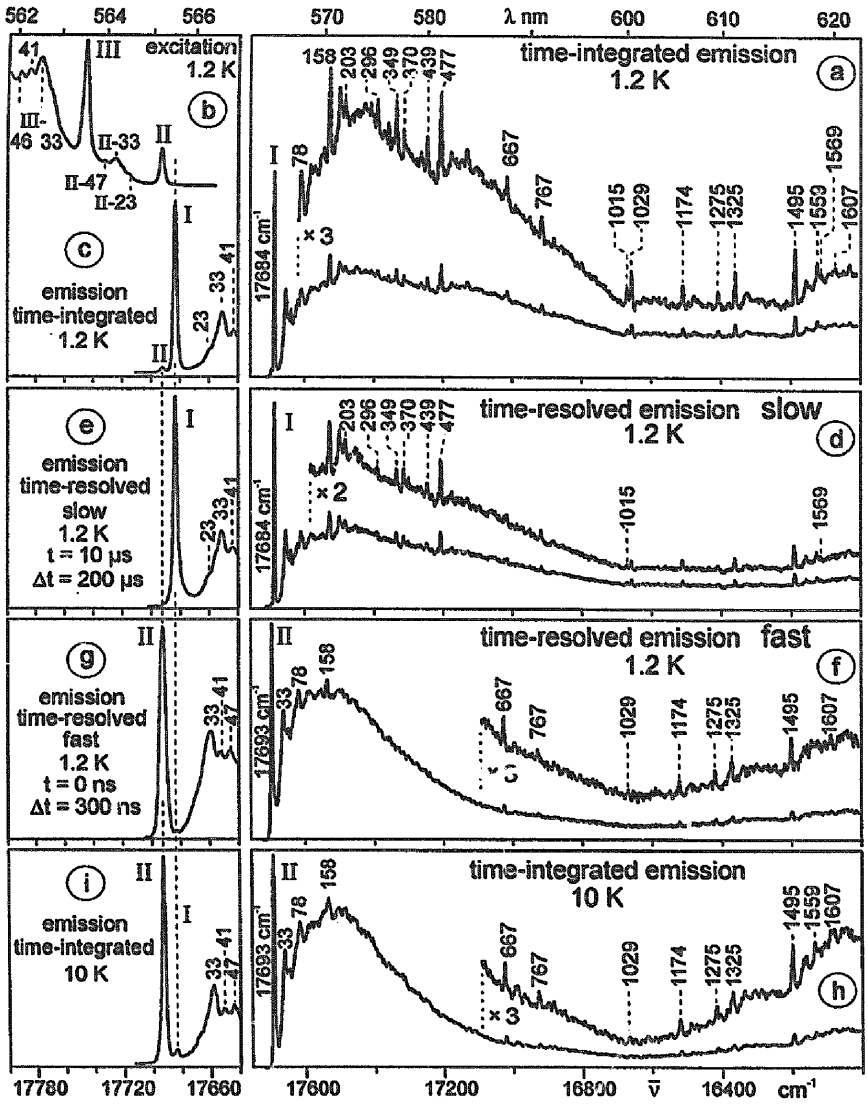

Fig. 9. Time-integrated and time-resolved emission and excitation spectra at $T = 1.2$ K and 10 K of $[Ru(bpy\text{-}h_8)_3]^{2+}$ in $[Zn(bpy\text{-}h_8)_3](ClO_4)_2$ (see Ref. [85]). The crystals were grown from water with a solution molar ratio Ru(II):Zn(II) of 0.5%. The emission was excited at 17 745 cm^{-1} (origin III), and the excitation spectrum (b) was detected at 17 207 cm^{-1} ($\triangleq$ 477 cm^{-1} satellite to origin I). The region of the electronic origins is reproduced on an enlarged scale. The energies of the vibrational and phonon satellites are given relative to the respective electronic origins. Satellites specified in the slow-decaying spectrum (d) represent HT acitve modes deactivating the transition from $|I\rangle$, while those modes specified in the fast-decaying emission from $|II\rangle$ (f) show FC activity (see Fig. 8). The drastic shift of the emission spectrum with time (compare (g) to (e) and (f) to (d)) is a consequence of the relatively slow spin–lattice relaxation and has nothing to do with a localization process.

vibrational and phonon satellite structure is observed. The lattice modes are easily identified (Fig. 9a, c). Their energies (relative to the electronic origin I) lie below $\approx 100\ cm^{-1}$, and since they are largely determined by the matrix, the same values are found for $[Os(bpy)_3]^{2+}$- (Table 2) and partly also for $[Rh(bpy)_3]^{3+}$-doped $[Zn(bpy\text{-}h_8)_3](ClO_4)_2$ (Table 1). In contrast to $[Rh(bpy)_3]^{3+}$

Table 2
Vibrational satellites (cm^{-1}) observed in the time-integrated and time-resolved emission spectra of $[Ru(bpy\text{-}h_8)_3]^{2+}$ in $[Zn(bpy\text{-}h_8)_3](ClO_4)_2$ ($T=1.2$ K)

Time-integrated emission $\|I\rangle \rightarrow \|0\rangle$ at 17 684 cm^{-1}	Time-resolved emission[a] slow: $t=10$ μs; $\Delta t=200$ μs $\|I\rangle \rightarrow \|0\rangle$ at 17 684 cm^{-1}	Time-resolved emission[b] fast: $t=0$ ns; $\Delta t=300$ ns $\|II\rangle \rightarrow \|0\rangle$ at 17 693 cm^{-1}	Assignments
23			Lattice mode[c]
33			Lattice mode[c,d]
41			Lattice mode[c]
47			Lattice mode[c,d]
56			Lattice mode[c]
66			Lattice mode[c]
78			Lattice mode[c]
158		158	FC[e]
296	296		M–L[f], HT[g]
349	349		M–L, HT, 349[h]
370	370		M–L, HT, 369[h]
420	420		M–L, HT, 419[h]
439	439		HT, 440[h]
477	477		HT, 474[h]
667		667	L[i], FC, 668[j,k]
767		767	FC, 765[j], 767[k]
1015	1015		HT, 1015[h]
1029		1029	FC, 1025[j], 1028[k]
1174		1174	FC, 1173[j], 1176[k]
1275		1275	FC, 1278[j], 1276[k]
1325		1325	FC, 1317[j], 1320[k]
1495		1495	FC, 1490[j], 1491[k]
1559			FC, 1558[j], 1563[k]
1569	1569		HT, 1567[h]
1607		1607	FC, 1607[j], 1608[k]

[a]Vibrational modes, selectively observed in the slow emission; from Fig. 9d.
[b]Vibrational modes dominating the fast emission; from Fig. 9f.
[c,d]Lattice modes detected in the same matrix doped with $[Os(bpy)_3]^{2+}$ (c) from [51] and $[Rh(bpy)_3]^{3+}$ (d) from Table 1.
[e]FC: Franck–Condon mode (see text).
[f]M–L: metal–ligand mode.
[g]HT: Herzberg–Teller mode (see text).
[h]IR active mode measured at 6 K [142].
[i]L: ligand mode. Modes above about 500 cm^{-1} are assigned to ligand vibrations [60,141].
[j]Raman active mode; from Ref. [141].
[k]Raman active mode; from Ref. [60].

and $[Pt(bpy)_2]^{2+}$, the satellites corresponding to the vibrational M–L modes (≈ 100 to $\approx 500\ cm^{-1}$) have significant intensities (compare with Section 5). The vibrational ligand modes are found above about 500 cm^{-1}. Moreover, there are satellites corresponding to combinations of vibrations with lattice modes and multiphonon bands. These are mainly responsible for the pronounced background.

Interestingly, no significant vibrational Franck–Condon progression is observed (Fig. 9a and Ref. [57]). The largest vibrational Huang–Rhys factor S [16,52,53] is of the order of 0.1. This value is even smaller than for $[Rh(bpy)_3]^{2+}$, with $S_{max} \approx 0.3$ (compare with Section 2.2.3). Thus, it follows that the ground $|0\rangle$ and excited state $|I\rangle$ have nearly identical nuclear equilibrium positions. Equivalent arguments also hold for the second (Fig. 9f, h) and third excited states [57]. Therefore, localization attributable to a strong distortion in these three states can be excluded (see Section 4.2 and Refs. [78,85]). Further evidence against such localization is presented in Section 4.3.2.

It is an important but not well-known fact that the lowest excited states $|I\rangle$ and $|II\rangle$ are not in fast thermal equilibrium at 1.2 K [78,85], owing to relatively slow phonon absorption and emission processes [53,129–132]. Thus, after excitation, e.g. into $|III\rangle$, state $|II\rangle$ is populated by a relatively fast relaxation process, but, owing to the low density of phonon states corresponding to the energy separation ΔE between $|II\rangle$ and $|I\rangle$, further relaxation down to $|I\rangle$ is strongly hindered (Fig. 8). This corresponds to a relatively long spin–lattice relaxation time τ(SLR). For $[Ru(bpy\text{-}h_8)_3]^{2+}$ in $[Zn(bpy\text{-}h_8)_3](ClO_4)_2$, a value of (220 ± 10) ns is found, as reported for the first time in Ref. [78]; compare also with Ref. [85]. Very recently, it has also been possible [132] to assign the effective mechanism of SLR at low temperatures ($T < 6$ K) to a *direct process* [53], while for $T > 6$ K the *Orbach process* [53,129–131] strongly grows in [132]. During the relaxation time, state $|II\rangle$ emits with the lifetime τ(SLR), depleting $|II\rangle$ but populating $|I\rangle$. Finally, state $|I\rangle$ emits with its usual emission lifetime of 230 μs (Fig. 8) The lifetime τ(SLR) of state $|II\rangle$ should not be mixed up with the emission lifetime, which is governed by radiative and non-radiative decays from state $|II\rangle$ into the ground state $|0\rangle$ of 8 μs [85] (see also Crosby and co-workers [18,95]). It should be mentioned that the processes of SLR had already been studied more than three decades ago, for example, for organic compounds [47–49,76,77] and for ruby [53,129–131]. However, the relevance of the spin–lattice relaxation for low-temperature emission spectra of transition metal complexes was emphasized only recently [22–25,42,78,85,132].

According to the discussion presented, the time-integrated low-temperature spectrum consists of superimposed emission spectra from $|I\rangle$ and $|II\rangle$ with, however, very different decay properties. Thus, it is expected that the spectra of these two states can be separated by time-resolved spectroscopy. This is indeed possible, as is shown in Fig. 9d–g). The *fast* spectra (Fig. 9f, g) are measured with no delay with respect to the exciting laser pulse ($t = 0$ ns) and integrated over a time window of $\Delta t = 300$ ns, while the slow emission, shown in Fig. 9d, e, is registered with a delay time of $\Delta t = 10$ μs and a time integration (time window) of $\Delta t = 200$ μs. These two spectra differ significantly in the region of the electronic origins (compare Fig. 9e to Fig. 9g [78]) and in a series of vibrational satellites (compare Fig. 9d to Fig. 9f).

Even at 1.2 K, the fast-decaying spectrum represents the emission from the higher-lying state |II⟩, while the slow-decaying one displays the emission from |I⟩. In the case of $[Ru(bpy)_3]^{2+}$, this slow spectrum is similar to the time-integrated emission at low temperature (compare Fig. 9a, c to Fig. 9d, e), since the relaxation from |II⟩ effectively populates |I⟩ (compare $Pd(2\text{-thpy})_2$ for a different behavior [23]). However, the fast-decaying spectrum from |II⟩ strongly resembles the time-integrated emission at $T = 10$ K (compare Fig. 9f, g to Fig. 9h, i). The processes of SLR become very fast with increasing temperature [23,24,47–49,53,129–132]. Consequently, at 10 K the system is largely thermalized, and the emission is determined by a Boltzmann distribution. This distribution displays the ratio (being ≈ 50) of the radiative decay rates of state |II⟩ relative to state |I⟩ (see Fig. 9b and e.g. Refs. [103] and [132]).

A comparison of the slow-decaying emission from |I⟩ to the fast-decaying spectrum from |II⟩ (Fig. 9d, f) clearly shows that the vibrational satellite structures differ significantly (Table 2). This behavior illustrates the different radiative decay mechanisms for these two states. Similar properties were recently discussed in detail for a series of other transition metal complexes [23,25,85,133,134]. According to these investigations and to the fact that the electronic transition $|0\rangle \leftrightarrow |II\rangle$ is allowed, albeit weakly, it follows that the radiative deactivation at the electronic origin is governed by direct spin–orbit coupling (see, for example, Ref. [135]). Thus, it can be concluded that the vibrational structure belonging to the transition $|II\rangle \leftrightarrow |0\rangle$ should consist mainly of totally symmetric FC fundamentals. Indeed, this is observed (Table 2, column 3). The electronic transition probability $|0\rangle \leftrightarrow |I\rangle$ is very small (long emission lifetime, no excitation peak, Fig. 9b). Therefore, radiative deactivation via vibronic HT coupling [135–137] becomes additionally important. It follows that those vibrational modes selectively found in the slow-decaying spectrum (specified in Fig. 9d and Table 2) can be assigned to HT modes (see Ref. [57]). The effective HT mechanism is very likely a spin–vibronic process, occurring by a change of spin–orbit coupling through a vibration and thus vibronically mixes higher-lying singlet state(s) to the lowest triplet sublevel (see, for example, Refs. [134–137]). Interestingly, the selectivity with respect to the occurrence of HT and FC modes, respectively, is much more obvious for $[Os(bpy)_3]^{2+}$-doped $[Ru(bpy)_3](PF_6)_2$ [85,133,134] (with high-symmetry sites [124]), and for $Pd(2\text{-thpy})_2$ [23] and $Pt(2\text{-thpy})_2$ [25] in *n*-octane. In conclusion, it should be emphasized that the spectral shift of the emission with time (Fig. 9d, f) has nothing to do with the process of localization, but is simply a consequence of the hindered relaxation (SLR) from state |II⟩ to |I⟩.

An assignment of the vibrational modes observed is, in part, possible using the normal coordinate analysis of Kincaid and co-workers [60,117]. These authors describe the vibrational properties of a (Ru-bpy) subunit. This model certainly displays neither the M–L modes nor their energies correctly, but it seems to be suitable for the high-energy ligand (L) modes, since in the complete $[Ru(bpy)_3]^{2+}$ complex the L modes of different bpy ligands do not exhibit any significant coupling, either through space or via the heavy central metal (see Section 2.3 and Refs. [138],

[139] and [140]) Thus, a vibrational analysis of the complete system would very probably give very similar results for these high-energy L modes.

4.3.2. Delocalization in $[Ru(bpy\text{-}h_8)_2(bpy\text{-}d_8)]^{2+}$. Comparison to $[Ru(bpy\text{-}h_8)_3]^{2+}$ and $[Ru(bpy\text{-}d_8)_3]^{2+}$

Fig. 10 reproduces the emission spectra of the section-title compounds. These spectra largely correspond to those published in Ref. [21], but in Fig. 10 they are line narrowed and therefore much better resolved. A comparison of the emission properties of the per-protonated and per-deuterated complexes shows that all the effects usually occurring on deuteration can be observed [51,57,58], i.e. specific red shifts of all vibrational energies (except phonons), a distinct increase in the emission lifetime of $|I\rangle$ from 230 to 310 μs [21], and a blue shift of the electronic origin I by 40 cm^{-1} [21,57] (see also Section 2.3).

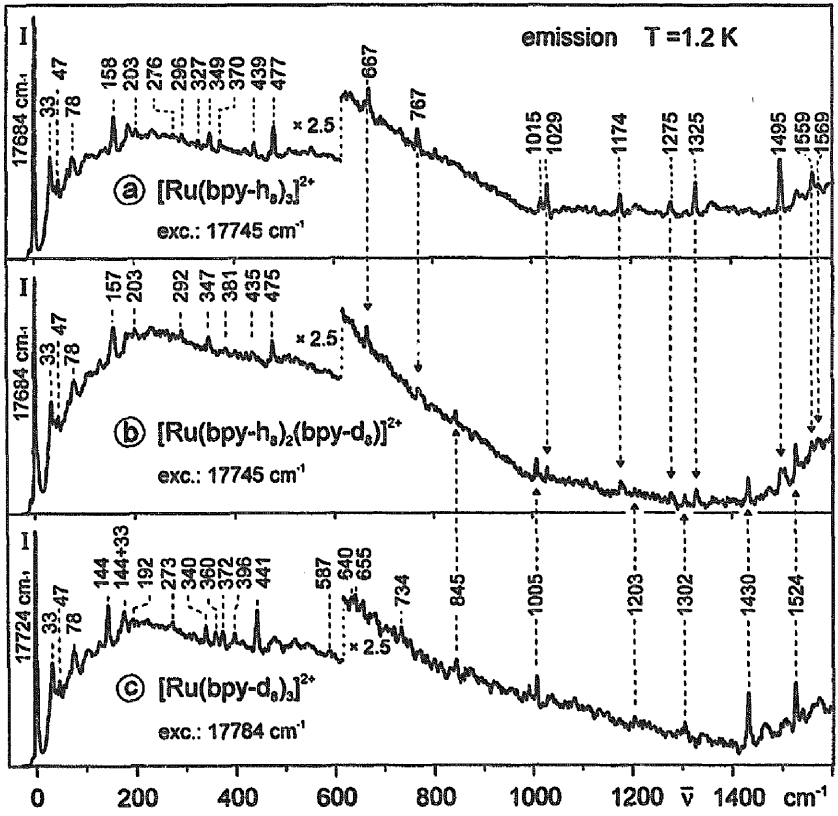

Fig. 10. Emission spectra of $[Ru(bpy\text{-}h_8)_3]^{2+}$, $[Ru(bpy\text{-}h_8)_2(bpy\text{-}d_8)]^{2+}$, and $[Ru(bpy\text{-}d_8)_3]^{2+}$ in $[Zn(bpy\text{-}h_8)_3](ClO_4)_2$ at $T = 1.2$ K (see Ref. [21]). The spectra are selectively excited into the respective electronic origins III. The wavenumber scale gives the separation from the lowest electronic origin I. For further data see Fig. 9. Note that $[Ru(bpy\text{-}h_8)_2(bpy\text{-}d_8)]^{2+}$ exhibits vibrational satellites, which correspond to both types of ligand. This is very strong evidence for delocalization in the lowest excited state.

Since neither the per-protonated nor the per-deuterated $[Ru(bpy)_3]^{2+}$ exhibits any obvious progression of vibrational modes, we can conclude that localization according to a *strong distortion* can be excluded (Section 4.2 and [57,78]). This is also valid for the partially deuterated complex [21]. Interestingly, the emission spectrum of $[Ru(bpy\text{-}h_8)_2(bpy\text{-}d_8)]^{2+}$ displays the delocalized situation even more obviously. This is clearly seen when focusing on the vibrational satellite structures in the range of the *high-energy ligand* modes ($\bar{\nu} > 600$ cm^{-1}) and when taking into account that (i) vibrational satellites only occur in electronic spectra if the corresponding ligand is electronically involved [21,26,27,51,143] and (ii) a significant coupling of these high-energy internal-ligand modes through space or via the heavy central metal can be excluded (see Section 2.3, Section 4.3.1, and Refs. [21,51,60,138–140,144]). Thus, it follows from the appearance of equally strong vibrational satellites corresponding to protonated *and* to deuterated ligands—belonging to the same electronic origin I (Fig. 10b)—that both ligands are involved in the electronically excited state $|I\rangle$. This means that state $|I\rangle$ is delocalized over the $(bpy\text{-}h_8)$ and $(bpy\text{-}d_8)$ ligands (and the metal). For completeness it is mentioned that this discrepancy is seen by the authors of Ref. [118], and is explained by introducing an additional electronic coupling between the ligands via the metal due to electronic backbonding effects [120], though the same authors excluded such a significant electronic coupling as the most crucial condition for their model of isolated (Ru-bpy) subunits. (See Section 4.2.2.). Moreover, if the lowest excited state is delocalized in $[Ru(bpy\text{-}h_8)_2(bpy\text{-}d_8)]^{2+}$, it will also be delocalized in both per-complexes. These conclusions may also be extended to the second and third excited state [21]. It should further be mentioned that hopping or tunneling processes between assumed localizations on different ligands does not describe the experimental observations correctly (for details see Refs. [21,51,85]).

It is very informative to discuss the excitation spectra too (Fig. 11). In the region of the electronic origins they can be well resolved by applying the technique of excitation line narrowing. This is easily achieved if the detection energy is chosen to select only a small spectral range of the inhomogeneously broadened emission of line I. Fig. 11a shows the line-narrowed excitation spectrum of $[Ru(bpy\text{-}h_8)_3]^{2+}$. The electronic origins II and III are clearly observed connected with a series of lattice mode satellites (see also Section 4.3.1). Both electronic origins are accompanied on their blue sides by spectrally broader features (halfwidths ≈ 3.7 cm^{-1}), which cannot be assigned to phonon satellites owing to their very small energy separations from the sharp origins (halfwidths ≈ 1.2 cm^{-1}). These broader features exhibit some peculiarities: (i) they disappear when detecting on the high-energy side of the inhomogeneously broadened line I; (ii) their relative intensities vary by a factor of at least two according to the selected area of the crystal, depending on whether deeply or only slightly red colored sections are chosen (inset Fig. 11a). The same behavior is found for the per-deuterated complex (Fig. 11c).

According to Section 4.1, it should be taken into account that the $[Ru(bpy)_3]^{2+}$ complexes in the $[Zn(bpy)_3](ClO_4)_2$ matrix are not statistically distributed. $[Ru(bpy)_3]^{2+}$ tends to form aggregates or nearest neighbor arrangements. Applying the technique of line narrowing, it is possible to select $[Ru(bpy\text{-}h_8)_3]^{2+}$ species in

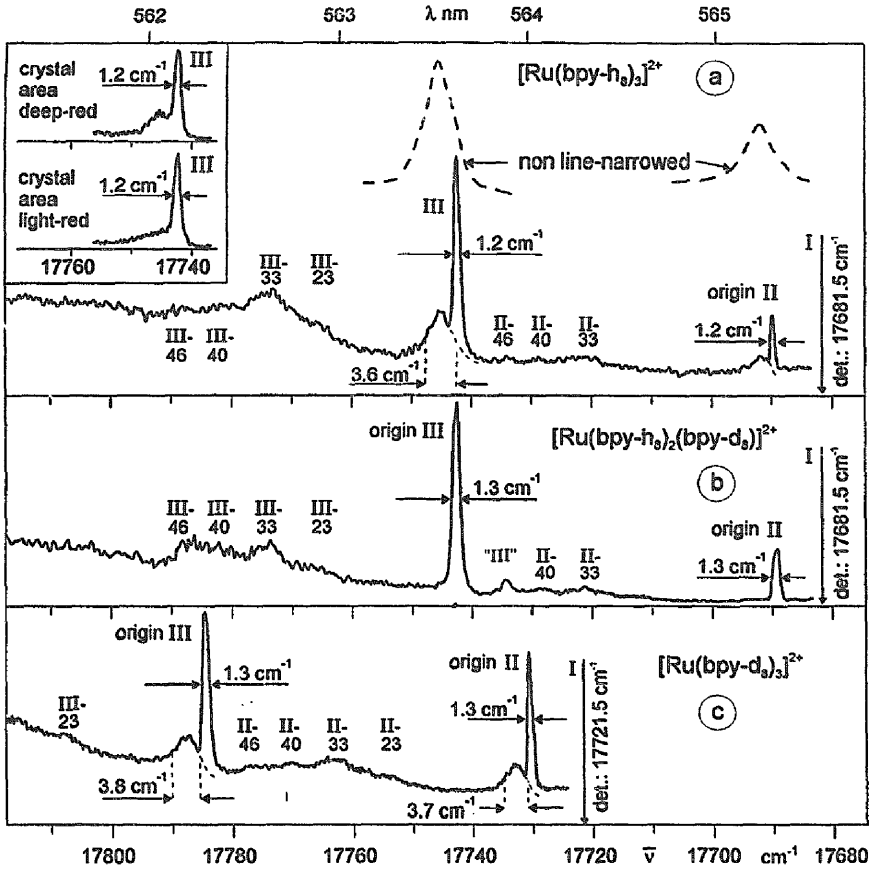

Fig. 11. Line-narrowed excitation spectra at $T=1.2$ K of $[Ru(bpy\text{-}h_8)_3]^{2+}$, $[Ru(bpy\text{-}h_8)_2(bpy\text{-}d_8)]^{2+}$, and $[Ru(bpy\text{-}d_8)_3]^{2+}$ in $[Zn(bpy\text{-}h_8)_3](ClO_4)_2$. The crystals were grown from aqueous solutions having molar ratios Ru(II):Zn(II) of 0.5% (a, b); 0.3% (c); 0.03% (inset). The spectra show the electronic origins II and III and the corresponding phonon satellites. Detection is at the energy of the respective electronic origin I. Peak "III" represents an unavoidable artefact; see text. Inset: the excitation structures of the electronic origin III (same cm^{-1} scale) measured at two positions of the same crystal. The spectral change displays the differences in clustering of the $[Ru(bpy)_3]^{2+}$ chromophores (see Section 4.1). It is important to note that $[Ru(bpy\text{-}h_8)_2(bpy\text{-}d_8)]^{2+}$ exhibits the same number of electronic origins as found for the per-compounds.

an equal environment, thus obtaining sharp origins. However, the selected species have nearest neighbors which are inhomogeneously distributed. Thus, if these neighbors are excited and if they transfer their excitation energy to the selected species, inhomogeneously broadened features may be observed on the blue sides of the sharp origins. The relative intensities and halfwidths of these broader features depend on the detection energy (lying within the inhomogeneous distribution of transition $|I\rangle \rightarrow |0\rangle$), on the individual (and unknown) nearest-neighbor arrangements, and on the efficiencies of radiationless energy transfer to the selected species. In a recent investigation [145], the importance of energy transfer between nearest neighbors

could be demonstrated for neat $[Ru(bpy\text{-}h_8)_3](PF_6)_2$. The transfer process between non-resonant neighbors in this compound is governed by a 60 ns process. Thus, it is also expected to find emission decay and/or rise times of this order of magnitude for the nearest-neighbor arrangements (clusters) discussed above. Indeed, such effects in a 20 ns time regime have been reported in Ref. [119] to occur for $[Ru(bpy)_3]^{2+}$ in $[Zn(bpy)_3](ClO_4)_2$. However, in Ref. [119] these effects are not ascribed to aggregates, but to slow processes of energy transfer between *different ligands of the same complex* (see below).

Fig. 11b reproduces the line-narrowed excitation spectrum of $[Ru(bpy\text{-}h_8)_2(bpy\text{-}d_8)]^{2+}$. The electronic origins of just the two lowest excited states $|II\rangle$ and $|III\rangle$ are clearly observed (and not four states as claimed in Refs. [118,119]), but the broader features on the blue sides of the sharp peaks are not detected for the crystals investigated. This behavior indicates that the partially deuterated complexes are built in differently into the $[Zn(bpy)_3](ClO_4)_2$ matrix compared to the per-complexes. This is not unexpected, according to Section 4.1. The occurrence of an additional peak, called "III" in Fig. 11b, might be surprising. It represents a peak resulting from an "artefact", which is necessarily connected with the procedure of measuring line-narrowed excitation spectra, when the inhomogeneous linewidth is broader than the energy separation between lines I and II (8.7 cm^{-1}, Fig. 8). This is the case for the partially deuterated complex in $[Zn(bpy\text{-}h_8)_3](ClO_4)_2$. By selecting a detection energy lying within the distribution of line I, it is impossible to avoid some residual emission intensity due to other complexes that have their emission line II at just that detection energy. Thus, the excitation peak "III" is connected to the emission due to line II, and it appears exactly 8.7 cm^{-1} below line III. Indeed, peak "III" displays the temperature (Fig. 9c, i) and time (Fig. 9e, g) behavior of state II emission. Consequently, its appearance may be disregarded.

4.3.3. $[Ru(bpy\text{-}h_8)_2(bpy\text{-}d_8)]^{2+}$ compared to $[Rh(bpy\text{-}h_8)_2(bpy\text{-}d_8)]^{3+}$

It is very instructive to compare the emission and excitation spectra of $[Ru(bpy\text{-}h_8)_2(bpy\text{-}d_8)]^{2+}$ to those of $[Rh(bpy\text{-}h_8)_2(bpy\text{-}d_8)]^{3+}$. As expected, both compounds show totally different behavior.

The Rh complex is well described by weakly interacting $LC^3\pi\pi^*$ states on different ligands (small *B* value), which are decoupled even by small distortions, and especially provoked by the deuteration of one ligand (Section 2.3). This has two principal consequences: (i) the emission stems exclusively from the energetically lower-lying *protonated* ligand(s), and thus high-energy vibrational modes of the *deuterated* ligand are not observable; (ii) the excitation spectrum shows quasi-superimposed spectra from *both* largely decoupled ($bpy\text{-}h_8$) and ($bpy\text{-}d_8$) ligands. It is emphasized that the electronic origins of the different ligands are clearly present (see Section 2.3 and Refs. [42,146]).

An exchange of the central metal ion from Rh^{3+} to Ru^{2+} may be regarded as "chemical tuning", which leads to significant ligand–ligand coupling via the metal d-orbitals. Thus, the lowest excited states of ^{3}MLCT character must be described by considering the whole strongly covalent complex with delocalized states. In particular, this has two consequences: (i) the emission spectrum (Fig. 10b) clearly

shows high-energy vibrational satellites of *both* (bpy-h_8) *and* (bpy-d_8) ligands, but connected to only one electronic state, i.e. the lowest excited state $|I\rangle$; (ii) the excitation spectrum does not exhibit separate electronic origins, corresponding to the different ligands, but shows exclusively the three expected electronic origins, as found for per-protonated and per-deuterated $[Ru(bpy)_3]^{2+}$.

For the sake of completeness, it is mentioned that the experimental results (i) and (ii) found for $[Ru(bpy\text{-}h_8)_2(bpy\text{-}d_8)]^{2+}$ contradict the model proposed by Riesen and co-workers [118–122]. Thus, it follows that their model of electronically nearly non-coupled ligands is neither applicable to $[Ru(bpy)_3]^{2+}$ nor consistent in itself.

5. Excited states, metal character, and covalency: a comparative conclusion

The lowest excited state of $[Rh(bpy)_3]^{3+}$ has been assigned to a ligand-centered $^3\pi\pi^*$ state. However, the relatively high probability of the $S_0 \rightarrow T_1$ transition, the decrease of emission lifetime by a factor of about 10^3 (both compared to the uncoordinated ligand [46]), and the occurrence of M–L vibrational satellites, albeit very weak ones, indicates (Section 2.2) the presence of an admixture of metal character to the lowest triplet, inducing an increase of spin–orbit coupling to higher-lying states. In this respect, the situation for $[Pt(bpy)_2]^{2+}$ is even more obvious (Section 3.2). Therefore, it is suitable to characterize the lowest triplet T_1 for these two systems as (see also Refs. [147] and [148])

$$|T_1\rangle = a|^3\pi\pi^*\rangle + b|^3d\pi^*\rangle + c|^3dd^*\rangle + d\,(\text{singlet admixtures}) \text{ with } a \gg b, c, d$$

The inclusion of dd* states for $[Rh(bpy)_3]^{3+}$ is reasonable, since it is expected that they lie only about 2×10^3 cm^{-1} [149] higher than the emitting triplet, while for $Pt(bpy)_2]^{2+}$ an admixture of MLCT character seems to be more significant, owing to its relatively low energy (Fig. 4).

At present, the degree of admixture of metal character to the lowest $^3\pi\pi^*$ states cannot be calculated, but it seems to be possible to develop a classification based on experiment, which allows the importance of this admixture to be signified with respect to a series of physical properties. This can be achieved by a comparison with bpy, on the one hand, and with $[Ru(bpy)_3]^{2+}$ and $[Os(bpy)_3]^{2+}$, on the other hand. Such a series is summarized in Table 3, where the compounds are arranged according to increasing importance of the metal character for the lowest excited and emitting states. Column (1) shows that the transition energies are red shifted with respect to the energy of the uncoordinated bpy. This stabilization results from the formation of the complex, and from increasing dd* and/or MLCT admixtures to the lowest ^{3}LC states of $[Rh(bpy)_3]^{3+}$ [42] and $[Pt(bpy)_2]^{2+}$ [75], while for $[Ru(bpy)_3]^{2+}$ and $[Os(bpy)_3]^{2+}$ the MLCT character becomes dominant [80–104,133,134]. (2) With increasing d-admixture and spin–orbit coupling, the spin selection rules are weakened. This leads to a significant increase of allowedness, and thus to a decrease of the lifetimes. (3) The ZFS does not seem to respond very sensitively to small dd* or MLCT admixtures, since total ZFS is nearly the same

Table 3
Comparison of spectroscopic properties for different 2,2'-bipyridine compounds[a]

Compound	(1) Lowest electronic transition[b] (cm^{-1})	(2) Emission lifetime[c] (μs)	(3) Zero-field splitting[d] (cm^{-1})	(4) $\frac{I(M-L\ vibr.)}{I(all\ vibr.)}$[e] (%)	(5) Huang–Rhys factor S[f]	(6) Deuteration-induced blue shift[g] (cm^{-1})	(7) Characterization of the electronic transition
bpy [54]in *n*-heptane	23 504	4×10^6 [46]	0.118 [46]	0	0.3	86	$^3\pi\pi^*$
$[Rh(bpy)_3]^{3+}$ [42] in $[Zn(bpy)_3](ClO_4)_2$	22 757	4.5×10^3	0.116 [40]	<0.5	0.3	61	$^3LC(\pi\pi^*)$ +small dd* admixtures[h]
$[Pt(bpy)_2]^{2+}$ [75] neat $[Pt(bpy)_2](ClO_4)_2$	21 237	50	—	2	0.3	≈50	$^3LC(\pi\pi^*)$ +small MLCT admixtures[h]
$[Ru(bpy)_3]^{2+}$ [21,57] in $[Zn(bpy)_3](ClO_4)_2$	17 684	230	61	40	0.1	40	$^3MLCT\ (d\pi^*)$
$[Os(bpy)_3]^{2+}$ [51] in $[Zn(bpy)_3](ClO_4)_2$	14 223	22	211	60	0.08	32	$^3MLCT\ (d\pi^*)$

[a]Data given for protonated compounds.
[b]Electronic origins being mainly of triplet character.
[c]Longest emission decay component at $T = 1.3$ K.
[d]Total zero-field splitting of the lowest triplet state.
[e]Ratio of the integrated intensities of vibrational satellites with significant M–L character relative to the intensity of all vibrational satellites (excluding lattice modes). For this rough estimate only M–L modes between ≈200 and ≈500 cm^{-1} were taken into account.
[f]Largest Huang–Rhys factor observed (see text).
[g]Blue shift of the electronic origin on per-deuteration.
[h]For a more detailed classification see Section 5.

for bpy [46] as for $[Rh(bpy)_3]^{3+}$ [30,39–41]. However, for MLCT states the ZFS becomes very large (Fig. 8). (4) An increasing d-contribution to the lowest excited LC states is equivalent to a larger spread of charge density into the molecular region between the metal and ligands. Thus, an electronic transition involving these states will also rearrange the charge density in that molecular region, leading to the occurrence of vibrational satellites of metal–ligand (M–L) character. A growing d-contribution is expected to lead to a larger intensity of M–L satellites [21,26,27]. Indeed, this effect occurs and is even more significant for MLCT transitions, as is clearly displayed in column (4) for the normalized intensities of M–L satellites. From column (5), it can be concluded that the nuclear equilibrium positions of the ground state and the lowest excited triplet state(s) are very similar for *all compounds*. This is manifested by the very small value of the Huang–Rhys factors S for all vibrational Franck–Condon modes (see Section 2.2.3, Section 4.3.1, and Refs. [42,57,134]). Interestingly, this property does not react very sensitively to small MLCT or dd* admixtures, but for compounds with ^{3}MLCT states, the S values become distinctly smaller still. This means that $[Ru(bpy)_3]^{2+}$ and $[Os(bpy)_3]^{2+}$ [51,134] have even less different equilibrium positions of the ground and excited states than $[Rh(bpy)_3]^{3+}$ or $[Pt(bpy)_2]^{2+}$. Moreover, column (6) shows that the deuteration-induced blue shifts of the lowest transitions also become distinctly smaller. Although this value represents only an average measure, it strongly indicates [57] the growing similarity of the vibrational force constants of the ground and lowest excited states for the compounds in the series presented. The tendencies shown in columns (5) and (6) simply display the increasing covalency in the series from $[Rh(bpy)_3]^{3+}$ to $[Os(bpy)_3]^{2+}$. Previously, before highly resolved spectra could be measured, this behavior was not expected for MLCT transitons. Finally, column (7) summarizes the rough classifications of the transitions discussed.

Interestingly, even a small d-admixture supplies enough electronic coupling between the different ligands in the partially deuterated Rh and Pt complexes to accomplish efficient interligand energy transfer from the deuterated to the protonated ligands. Thus, *only* an emission from the energetically lower-lying protonated ligands is observed (Section 2.4). However, this coupling between the triplets on different ligands seems to be far too small to delocalize the excitation energy in the sense of a "molecular excitation". Presumably, the coupling energy is much smaller than the inhomogeneous broadenings experienced by the triplets confined to the different ligands. In contrast, $[Ru(bpy)_3]^{2+}$ [21,85] and $[Os(bpy)_3]^{2+}$ [51,85] exhibit a strong electronic coupling, induced by the interactions via the metal. This leads to a strongly covalent and delocalized situation for the lowest excited ^{3}MLCT states being delocalized over the metal and the different ligands (Section 4.3). It is emphasized that neither of the currently discussed models of localization on one of the ligands—according to a *weak* or a *strong* distortion—are applicable to $[Ru(bpy)_3]^{2+}$ and $[Os(bpy)_3]^{2+}$ doped into the rigid $[Zn(bpy)_3](ClO_4)_2$ matrix.

Acknowledgements

Financial support of the "Deutsche Forschungsgemeinschaft" is gratefully acknowledged. We also thank Degussa AG (Hanau) for the donation of Rh, Ru,

and Os salts. Further, we thank Professor Dr. W.P. Griffith (Imperial College, London) and the University of London Intercollegiate Research Service (ULIRS) for giving us the opportunity to measure the Raman spectra. Dr. U. Rosellen (Düsseldorf) is acknowledged for allowing us to use IR data prior to publication.

References

[1] J.M. Lehn, Supramolecular Chemistry, Verlag Chemie, Weinheim, 1995.
[2] V. Balzani and F. Scandola, Supramolecular Chemistry, Horwood, Chichester, 1991.
[3] B. O'Regan and M. Grätzel, Nature, 353 (1991) 737.
[4] A. Juris, V. Balzani, F. Barigelletti, S. Campagna, P. Belser and A. von Zelewsky, Coord. Chem. Rev., 84 (1988) 85.
[5] T.J. Meyer, Acc. Chem. Res., 22 (1989) 163.
[6] V. Goulle, A. Harriman and J.M. Lehn, J. Chem. Soc. Commun., (1993) 1034.
[7] D.L. Ross and J. Blanc, Adv. Chem. Ser., 71 (1967) 155.
[8] (a) T.J. Maede and J.F. Kayyem, Angew. Chem., 107 (1995) 358.(b) R.E. Holmin and G.K. Barton, Inorg. Chem., 34 (1995) 7.
[9] (a) B. Wappes, M. Jennerwein, E. v. Angerer, H. Schönenberger, J. Engel, M. Berger and K.-H. Wrobel, J. Med. Chem., 27 (1984) 1280.(b) R. Gust, H. Schönenberger, J. Kritzenberger, K.-J. Range, U. Klement and T. Burgemeister, Inorg. Chem., 32 (1993) 5939.
[10] J. Kritzenberger, H. Yersin, M. Zabel and K.-J. Range, Inorg. Chim. Acta, 209 (1993) 77.
[11] J. Kritzenberger, G. Bernhardt, R. Gust, P. Pistor, H. Schönenberger and H. Yersin, Monatsh. Chem., 124 (1993) 587.
[12] H. Yersin and A. Vogler (Eds.), Photochemistry and Photophysics of Coordination Compounds, Springer Verlag, Berlin, 1987.
[13] H. Yersin (Ed.), Electronic and Vibronic Spectra of Transition Metal Complexes, Vol. I, Topics in Current Chemistry, Vol. 171, Springer Verlag, Berlin, 1994.
[14] S.P. McGlynn, T. Azumi and M. Kinoshita, Molecular Spectroscopy of the Triplet State, Prentice Hall, Englewood Cliffs, NJ, 1969.
[15] H.L. Schläfer and G. Cliemann, Basic Principles of Ligand Field Theory, Wiley-Interscience, London, 1969.
[16] E.I. Solomon, Comments Inorg. Chem., 3 (1984) 225–320.
[17] A.B.P. Lever, Inorganic Spectroscopy, Elsevier, Amsterdam, 1984.
[18] G.A. Crosby, Acc. Chem. Res., 8 (1975) 231.
[19] T.J. Meyer, Pure and Appl. Chem., 58 (1986) 1193.
[20] M. Maestri, V. Balzani, C. Deuschel-Cornioley and A. von Zelewsky, Adv. Photochem., 17 (1992) 1.
[21] D. Braun, P. Huber, J. Wudy, J. Schmidt and H. Yersin, J. Phys. Chem., 98 (1994) 8044.
[22] H. Yersin, S. Schützenmeier, H. Wiedenhofer and A. von Zelewsky, J. Phys. Chem., 97 (1993) 13 496.
[23] J. Schmidt, H. Wiedenhofer, A. von Zelewsky and H. Yersin, J. Phys. Chem., 99 (1995) 226.
[24] D. Becker-Donges, H. Yersin and A. von Zelewsky, Chem. Phys. Lett., 235 (1995) 490.
[25] H. Wiedenhofer, S. Schützenmeier, A. von Zelewsky and H. Yersin, J. Phys. Chem., 99 (1995) 13 385.
[26] H. Yersin, H. Wiedenhofer, P. Huber and D. Braun, 29th Int. Conference on Coordination Chemistry, Lausanne, Book of Abstracts, 1992, p. 53.
[27] H. Yersin, P. Huber and H. Wiedenhofer, Coord. Chem. Rev., 132 (1994) 35.
[28] G.A. Crosby and W.H. Elfring, Jr., J. Phys. Chem., 97 (1976) 2206.
[29] M. Nishizawa, T.M. Suzuki, S. Sprouse, R.J. Watts and P.C. Ford, Inorg. Chem., 23 (1984) 1837.
[30] A.L. Kamyshny, A.P. Suisalu and L.A. Aslanov, Coord. Chem. Rev., 117 (1992) 1.
[31] W. Halper and M.K. DeArmond, J. Lumin., 5 (1972) 225.

[32] The molecular exciton model is developed in analogy to Davydov theory, which is commonly used to describe dipole– dipole interactions and exciton band splittings in molecular crystals, e.g. see next reference.
[33] D.P. Craig and S.H. Walmsley, Excitons in Molecular Crystals, W.A. Benjamin, New York, 1968.
[34] S.F. Mason, Inorg. Chim. Acta Rev., 2 (1968) 89.
[35] A.J. McCaffery, S.F. Mason and B.J. Norman, J. Chem. Soc. A, (1969) 1428.
[36] B. Bosnich, in F. Ciardelli and P. Salvadori (Eds.), Fundamental Aspects and Recent Developments in Optical Rotary Dispersion and Circular Dichroism, Proc. NATO ASI, Heyden, London, 1971, p. 240.
[37] J.R. Watts and J. Van Houten, J. Am. Chem. Soc., 100 (1978) 1718.
[38] J. Westra and M. Glasbeek, J. Lumin., 53 (1992) 92.
[39] Y. Komada, S. Yamauchi and N. Hirota, J. Phys. Chem., 90 (1986) 6425.
[40] J. Westra and M. Glasbeek, Chem. Phys. Lett., 166 (1990) 535.
[41] J. Westra and M. Glasbeek, Chem. Phys. Lett., 180 (1991) 41.
[42] W. Humbs and H. Yersin, Inorg. Chem., 35 (1996) 2220.
[43] A. Zilian and H.U. Güdel, Inorg. Chem., 31 (1992) 830.
[44] A. Zilian and H.U. Güdel, J. Lumin., 51 (1992) 237.
[45] A. Zilian, G. Frei and H.U. Güdel, Chem. Phys., 173 (1993) 513.
[46] N. Okabe, T. Ikeyama and T. Azumi, Chem. Phys. Lett., 165 (1990) 24.
[47] D.S. Tinti and M.A. El-Sayed, J. Chem. Phys., 54 (1971) 2529.
[48] M.A. El-Sayed, in E.C. Lim (Ed.), Excited States, Vol. I, Academic Press, New York, 1974, p. 35.
[49] J. Fünfschilling (Ed.), Relaxation Processes in Molecular Excited States, Kluwer Academic, Dordrecht, 1989.
[50] D. Becker-Donges, J.K. Nagle and H. Yersin, Book of Abstracts, 11th Int. Symp. on the Photochemistry and Photophysics of Coordination Compounds, Krakow, 1995, p. 62.
[51] P. Huber and H. Yersin, J. Phys. Chem., 97 (1993) 12705.
[52] R.G. Denning, in C.D. Flint (Ed.), Vibronic Processes in Inorganic Chemistry, Mathematical and Physical Sciences, Vol. 288, Kluwer Academic, Dordrecht, 1989, p. 111.
[53] B. Henderson and G.F. Imbusch, Optical Spectroscopy of Inorganic Solids, Clarendon Press, Oxford, 1989.
[54] P. Huber, PhD Thesis, Universität Regensburg, 1994.
[55] R.B. Wilson and E.I. Solomon, J. Am. Chem. Soc., 102 (1980) 4085.
[56] D. Wexler, J.I. Zink and C. Reber, in H. Yersin (Ed.), Electronic and Vibronic Spectra of Transition Metal Complexes, Vol. I, Topics in Current Chemistry, Vol. 171, Springer Verlag, Berlin, 1994, p. 173.
[57] H. Yersin and D. Braun, Chem. Phys. Lett., 179 (1991) 85.
[58] H. Yersin, P. Huber and D. Braun, J. Phys. Chem., 94 (1990) 3560.
[59] M.R. Wright, R.P. Frosch and G.W. Robinson, J. Chem. Phys., 33 (1960) 934.
[60] P.K. Mallick, G.D. Danzer, D.P. Strommen and J.R. Kincaid, J. Phys. Chem., 92 (1988) 5628.
[61] K. Maruszewski, K. Bajdor, D.P. Strommen and J.R. Kincaid, J. Phys. Chem., 99 (1995) 6286.
[62] M.G. Colombo, A. Hauser and H.U. Güdel, in H. Yersin (Ed.), Electronic and Vibronic Spectra of Transition Metal Complexes, Vol. I, Topics in Current Chemistry, Vol. 171, Springer Verlag, Berlin, 1994, p. 143.
[63] E. Krausz, J. Higgins and H. Riesen, Inorg. Chem., 32 (1993) 4053.
[64] M.G. Colombo, A. Hauser and H.U. Güdel, Inorg. Chem., 32 (1993) 3088.
[65] (a) G. Gliemann and H. Yersin, Struct. Bonding (Berlin), 62 (1985) 87.(b) H. Yersin, Habilitation, Universität Regensburg, 1979.
[66] H. Yersin and U. Riedl, Inorg. Chem., 34 (1995) 1642.
[67] V.H. Houlding and V.M. Miskowksi, Coord. Chem. Rev., 111 (1991) 145.
[68] V.M. Miskowski and V.H. Houlding, Inorg. Chem., 28 (1989) 1529.
[69] L.V. Interrante, Extended Interactions between Metal Ions in Transition Metal Complexes, ACS Symp. Ser. 5, American Chemical Society, Washington, DC, 1974.
[70] D.L. Webb and L.A. Rossiello, Inorg. Chem., 10 (1971) 2213.

[71] M. Maestri, D. Sandrini, V. Balzani, A. von Zelewsky, C. Deuschel-Cornioley and P. Jolliet, Helv. Chim. Acta, 71 (1988) 1053.
[72] G. Nord, Acta Chem. Scand., Ser. A, 29 (1975) 270.
[73] S.C. Dkhara, M.I. Gel'fman and Y.N. Kukushkin, Zh. Neorg. Khim., 13 (1968) 2550.
[74] K.P. Balashev, A.M. Zimnyakov and S.A. Vinogradov, Zh. Fiz. Khim., 62 (1988) 1635.
[75] W. Humbs and H. Yersin, Book of Abstracts, 11th Int. Symp. on the Photochemistry and Photophysics of Coordination Compounds, Krakow, 1995, p. 69.
[76] S. Yamauchi and T. Azumi, Chem. Phys. Lett., 21 (1973) 603.
[77] F. Kokai and T. Azumi, J. Chem. Phys., 77 (1982) 2757.
[78] H. Yersin and D. Braun, Coord. Chem. Rev., 111 (1991) 39.
[79] For $[Rh(bpy)_3]^{3+}$, the 545 and 746 cm^{-1} modes seem to be HT active with respect to the radiative deactivation of state $|I\rangle$; see W. Humbs, Diplomarbeit, Universität Regensburg, 1994.
[80] P. Belser, Chemia, 44 (1990) 226.
[81] R.A. Krause, Struct. Bonding (Berlin), 67 (1987) 2.
[82] E. Krausz and J. Ferguson, Progr. Inorg. Chem., 37 (1989) 293.
[83] H. Yersin, D. Braun, G. Hensler and E. Gallhuber, in C.D. Flint (Ed.), Vibronic Processes in Inorganic Chemistry, Kluwer Academic, Dordrecht, 1989, p. 195.
[84] E. Krausz, Comments Inorg. Chem., 7 (1988) 139.
[85] H. Yersin, W. Humbs and J. Strasser, in H. Yersin (Ed.), Electronic and Vibronic Spectra of Transition Metal Complexes, Vol. II, Topics in Current Chemistry 191, Springer Verlag, Berlin, 1997.
[86] H.D. Gafney, Coord. Chem. Rev., 104 (1990) 113.
[87] D.M. Roundhill, Photochemistry and Photophysics of Metal Complexes, Plenum, New York, 1994, p. 165.
[88] L.E. Orgel, J. Chem. Soc., (1961) 3683.
[89] A. Ceulemans and L.G. Vanquickenborne, J. Am. Chem. Soc., 103 (1981) 2238.
[90] E.M. Kober and T.J. Meyer, Inorg. Chem., 21 (1982) 3967.
[91] F. Felix, J. Ferguson, H.U. Güdel and A. Ludi, J. Am. Chem. Soc., 102 (1980) 4096.
[92] C. Daul and C.W. Schlaepfer, J. Chem. Soc., Dalton Trans., (1988) 393.
[93] C. Daul, E.J. Baerends and P. Vernooijs, Inorg. Chem., 33 (1994) 3538.
[94] G. Calzaferri and R. Rytz, J. Phys. Chem., 99 (1995) 12 141.
[95] G.D. Hager, R.J. Watts and G.A. Crosby, J. Am. Chem. Soc., 97 (1975) 7037, 7031.
[96] H. Yersin, E. Gallhuber, A. Vogler and H. Kunkely, J. Am. Chem. Soc., 105 (1983) 4155.
[97] H. Yersin and E. Gallhuber, J. Am. Chem. Soc., 106 (1984) 6582.
[98] H. Yersin, E. Gallhuber and G. Hensler, Chem. Phys. Lett., 134 (1987) 497.
[99] T. Schönherr, J. Degen, E. Gallhuber, G. Hensler and H. Yersin, Chem. Phys. Lett., 158 (1989) 519.
[100] M. Kato, S. Yamauchi and N. Hirota, Chem. Phys. Lett., 157 (1989) 543.
[101] H. Yersin, E. Gallhuber and G. Hensler, J. Phys., Colloq. C 7 (Suppl.), 46 (1985) C7–453.
[102] E. Gallhuber, G. Hensler and H. Yersin, Chem. Phys. Lett., 120 (1985) 445.
[103] G. Hensler, E. Gallhuber and H. Yersin, Inorg. Chim. Acta, 113 (1986) 91.
[104] H. Yersin, G. Hensler and E. Gallhuber, Inorg. Chim. Acta, 132 (1987) 187.
[105] (a) W. Kleber, Einführung in die Kristallographie, Verlag Technik, Berlin, 1983, p. 195.(b) F. Rosenberger, Fundamentals of Crystal Growth I, Springer Ser. Solid State Sci., 5 (1979) 395.
[106] E. Krausz, H. Riesen and A.D. Rae, Aust. J. Chem., 48 (1995) 929.
[107] U. Klement, D. Trümbach and H. Yersin, Z. Kristallogr., 210 (1995) 228.
[108] J.M. Harrofield and A. N. Sobolev, Aust. J. Chem., 47 (1994) 763.
[109] Y. Toyozawa, in P. Reinecker, H. Haken and H.C. Wolf (Eds.), Organic Molecular Aggregate, Springer Ser. Solid State Sci., 49 (1983) 90.
[110] (a) P.W. Atkins, Molecular Quantum Mechanics, Oxford University Press, 1983.(b) K.Y. Wong and P.N. Schatz, Progr. Inorg. Chem., 28 (1981) 369.
[111] J. Jortner, S.A. Rice, J.L. Katz and S.-I. Choi, J. Chem. Phys., 42 (1965) 309.
[112] A.H. Francis and C.B. Harris, Chem. Phys. Lett., 9 (1971) 181, 188.
[113] R. Schmidberger and H.C. Wolf, Chem. Phys. Lett., 16 (1972) 402.
[114] D.D. Dlott and M.D. Fayer, Chem. Phys. Lett., 41 (1976) 305.

[115] P.G. Bradley, N. Kress, B.A. Hornberger, R.F. Dallinger and W.H. Woodruff, J. Am. Chem. Soc., 103 (1981) 7441.
[116] M. Forster and R.E. Hester, Chem. Phys. Lett., 81 (1981) 42.
[117] D.P. Strommen, P.K. Mallick, G.D. Danzer, R.S. Lumpkin and J.R. Kincaid, J. Phys. Chem., 94 (1990) 1357.
[118] H. Riesen and E. Krausz, J. Chem. Phys., 99 (1993) 7614.
[119] H. Riesen, Y. Gao and E. Krausz, Chem. Phys. Lett., 228 (1994) 610.
[120] H. Riesen and E. Krausz, Comments Inorg. Chem., 18 (1995) 27.
[121] H. Riesen and E. Krausz, Chem. Phys. Lett., 212 (1993) 347.
[122] H. Riesen, A.D. Rae and E. Krausz, J. Lumin., 62 (1994) 123.
[123] Y. Komada, S. Yamauchi and N. Hirota, J. Phys. Chem., 92 (1988) 6511.
[124] M. Biner, H.-B. Bürgi, A. Ludi and C. Röhr, J. Am. Chem. Soc., 114 (1992) 5197.
[125] H. Yersin, E. Gallhuber, G. Hensler and D. Schweitzer, Chem. Phys. Lett., 161 (1989) 315.
[126] D. Braun, E. Gallhuber and H. Yersin, Chem. Phys. Lett., 171 (1990) 122; D. Braun, E. Gallhuber and H. Yersin, Chem. Phys. Lett., 173 (1990) 132.
[127] E. Krausz and G. Moran, J. Lumin., 42 (1988) 21.
[128] D. Trümbach, PhD Thesis, Universität Regensburg, 1995/1996.
[129] P.L. Scott and C.D. Jeffries, Phys. Rev., 127 (1962) 32.
[130] C.B.P. Finn, R. Orbach and W.P. Wolf, Proc. Phys. Soc. (London), 77 (1961) 261.
[131] S. Geschwind, G.E. Devlin, R.L. Cohen and S.R. Chinn, Phys. Rev. A, 137 (1965) 1087.
[132] H. Yersin and J. Strasser, J. Lumin., (1997) in press.
[133] D. Braun, E. Gallhuber, G. Hensler and H. Yersin, Mol. Phys., 67 (1989) 67.
[134] D. Braun, G. Hensler, E. Gallhuber and H. Yersin, J. Phys. Chem., 95 (1991) 1067.
[135] G. Fischer, Vibronic Coupling, Academic Press, London, 1984.
[136] A.C Albrecht, J. Chem. Phys., 38 (1963) 354.
[137] G. Fischer and A.E.W. Knight, Chem. Phys., 168 (1992) 211.
[138] J. Weidlein, U. Müller and K. Dehnicke, Schwingungsspektroskopie, Georg Thieme Verlag, Stuttgart, 1982, p. 52.
[139] K. Nakamoto, Infrared and Raman Spectra of Inorganic and Coordination Compounds, Wiley, New York, 1978, p. 197.
[140] N. Mohan, S.J. Cyvin and A. Müller, Coord. Chem. Rev., 21 (1976) 221.
[141] O. Poizat and C. Sourisseau, J. Phys. Chem., 88 (1984) 3007.
[142] U. Rosellen, unpublished results, 1991, University of Düsseldorf.
[143] C.J. Ballhausen, Molecular Electronic Structures of Transition Metal Complexes, McGraw-Hill, New York, 1979.
[144] E.A. Gastilovich, Sov. Phys. Usp., 34 (1991) 592.
[145] D. Braun and H. Yersin, Inorg. Chem., 34 (1995) 1967.
[146] W. Humbs, J. Strasser and H. Yersin, J. Lumin., (1997) in press.
[147] H. Miki, M. Shimada, T. Azumi, J.A. Brozik and G.A. Crosby, J. Phys. Chem., 97 (1993) 11 175.
[148] T. Azumi and H. Miki, in H. Yersin (Ed.), Electronic and Vibronic Spectra of Transition Metal Complexes, Vol. II, Topics in Current Chemistry 191, Springer Verlag, Berlin, 1997.
[149] F. Bolletta, A. Rossi, F. Barigelletti, S. Dellonte and V. Balzani, Gazetta Chim. Ital., 111 (1981) 155.